DOI: 10.1002/chem.200500548

Rationally Designed, Polymeric, Extended Metal–Ciprofloxacin Complexes

Dong-Rong Xiao,[a] En-Bo Wang,*[a] Hai-Yan An,[a] Zhong-Min Su,*[b] Yang-Guang Li,[a] Lei Gao,[a] Chun-Yan Sun,[a] and Lin Xu[a]

Abstract: Reactions of the antimicrobial fluoroquinolone ciprofloxacin (cfH) with metal salts in the presence of aromatic polycarboxylate ligands or under basic conditions produce fourteen new metal–cfH complexes, namely, $[Ba_2(cf)_2(1,4\text{-bdc})(H_2O)_2]\cdot H_2O$ (**1**), $[Sr_6(cf)_6(1,4\text{-bdc})_3(H_2O)_6]\cdot 2H_2O$ (**2**), $[M_2(cfH)_2(bptc)(H_2O)_2]\cdot 8H_2O$ (M = Mn(**3**) and Cd(**4**)), [M(cfH)(1,3-bdc)] (M = Mn(**5**), Co(**6**), and Zn(**7**)), $[Zn_2(cfH)_4(1,4\text{-bdc})](1,4\text{-bdc})\cdot 13H_2O$ (**8**), $[Ca(cfH)_2(1,2\text{-Hbdc})_2]\cdot 2H_2O$ (**9**) and $[M(cf)_2]\cdot 2.5H_2O$ (M = Mn(**10**), Co(**11**), Zn(**12**), Cd(**13**), and Mg(**14**)) (1,4-bdc = 1,4-benzenedicarboxylate, bptc = 3,3′,4,4′-benzophenonetetracarboxylate, 1,3-bdc = 1,3-benzenedicarboxylate, 1,2-bdc = 1,2-benzenedicarboxylate). Their structures were determined by single-crystal X-ray diffraction analyses and further characterized by elemental analyses, IR spectra, and thermogravimetric analyses. The structures of **1** and **2** consist of unique two-dimensional arm-shaped layers. Compounds **3** and **4** are isostructural and feature one-dimensional structures formed from the interconnection of $[M_2(cfH)_2(H_2O)_2]$ dimers with bptc ligands. Compounds **5–7** are isostructural and contain double-chain-like ribbons constructed from $[M_2(cfH)_2(CO_2)_2]$ dimers and 1,3-bdc. Compound **8** consists of a pair of $[Zn(cfH)_2]^{2+}$ fragments bridged by a 1,4-bdc into a dinuclear dumbbell structure. Compound **9** is a neutral monomeric complex. To the best of our knowledge, compounds **1–9** are the first examples of metal-quinolone complexes that contain aromatic polycarboxylate ligands. Compounds **10–14** are isostructural and exhibit interesting two-dimensional rhombic grids featuring large cavities with dimensions of 13.6 × 13.6 Å. Up to now, polymeric extended metal–cfH complexes have never been reported.

Keywords: ciprofloxacin · coordination polymers · hydrothermal synthesis · N ligands · structure elucidation

Introduction

The design and synthesis of metal-organic coordination networks have undergone revolutionary growth over the past decade, not only because of their intriguing structural diversity but also because of their tremendous potential applications in catalysis, molecular adsorption, magnetism, nonlinear optics, and molecular sensing.[1–3] A series of attractive networks with various structural motifs, including honeycomb, brick wall, bilayer, ladder, herringbone, diamondoid, and rectangular grid, have been deliberately designed, and extensively discussed in comprehensive reviews by Yaghi, Kitagawa, Rao, Chen, and their co-workers.[4] It should be noted that, to date, aromatic polycarboxylate and neutral organonitrogen ligands, such as 1,4-benzenedicarboxylate, 1,3,5-benzenetricarboxylate, 1,2,4-benzenetricarboxylate, 1,2,4,5-benzenetetracarboxylate, 4,4′-bpy, and pyrazine, have been widely used in the construction of these high-dimensional structures with large pores or undulating layers.[5–9] The construction of metal-organic coordination frameworks using organic drugs is still in its infancy, although many organic drugs have the potential to act as building blocks, and the resulting metal-drug complexes are particularly important in biology and pharmacology.[10–12]

Ciprofloxacin (cfH = 1-cyclopropyl-6-fluoro-1,4-dihydro-4-oxo-7-(1-piperazinyl)-3-quinoline carboxylic acid) (Scheme 1), a fluoroquinolone antibacterial agent with a

[a] Dr. D.-R. Xiao, Prof. E.-B. Wang, Dr. H.-Y. An, Dr. Y.-G. Li, L. Gao, C.-Y. Sun, Prof. L. Xu
Institute of Polyoxometalate Chemistry
Department of Chemistry, Northeast Normal University
Changchun 130024 (China)
Fax: (+86) 431-509-8787
E-mail: wangenbo@public.cc.jl.cn

[b] Prof. Z.-M. Su
Institute of Functional Materials
Department of Chemistry, Northeast Normal University
Changchun, Jilin, 130024 (China)
E-mail: zmsu@nenu.edu.cn

Supporting information for this article is available on the WWW under http://www.chemeurj.org/ or from the author.

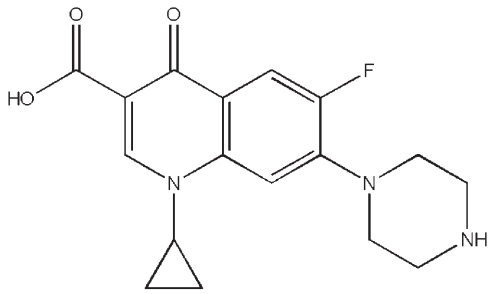

Scheme 1. Structure of ciprofloxacin.

wide spectrum of activity, is extremely useful for the treatment of a variety of infections.[13–14] The mechanisms of action of the quinolone antibacterial agents are either their inhibition of DNA gyrase (topoisomerase II), an essential bacterial enzyme that maintains superhelical twists in DNA, or their interaction with the DNA molecule via a metal–complex intermediate.[11–16] In fact, the chelation between the metal and the carbonyl and carboxyl groups of the quinolones and the binding of the resulting complex to DNA may be the essential prerequisites for their antibacterial activity.[11,17] Recently new theoretical/experimental studies on the activity of quinolones and their metal complexes have supported the hypothesis that the mechanism of action of quinolones could be mediated by a metal ion.[14,18] Despite the important role that metal ions may play in this system, the structurally characterized metal–cfH complexes are still rare, as evidenced in a recent review by Turel.[14] Only a few zero-dimensional monomeric structures have been characterized to date.[15,16] However, to the best of our knowledge, a polymeric extended metal–cfH complex has never been reported, which may be attributed to the fact that the bulky cf ligand play a "passive" role by occupying coordination sites on the metal centers and providing steric constraints, thus preventing spatial extension of the skeleton to higher dimensions. Therefore, searching for feasible routes to construct polymeric extended metal–cfH complexes is still a great challenge for synthetic chemists, and further research is necessary to enrich and develop this field.

Two different synthetic strategies were used in this paper to obtain polymeric extended metal–cfH complexes. In the first strategy, aromatic polycarboxylate ligands were used to link the discrete metal–cfH motif to form high-dimensional structures. Aromatic polycarboxylates are introduced based on the following considerations: 1) the use of carboxylate-bridged metal clusters as metal-organic second building units (SBUs) to build polymeric extended structures is relatively mature.[19] 2) The topologies of the resulting structures can be predicted and thus designed by the use of symmetrical aromatic polycarboxylates.[5] 3) No metal complexes containing mixed quinolone and aromatic polycarboxylate ligands have been reported.[14] The possible reason is that two carboxyl-containing ligands would yield more negative charges that would hamper charge balancing. 4) The combination of cfH and polycarboxylates may lead to the formation of unprecedented structures with novel topological features. The second strategy uses the cf as a bridging ligand under suitable reaction conditions. Owing to its distinct steric conformations, the piperazinyl group of cf usually acts as charge-compensating cation but rarely as a ligand to connect metals. However, recent work published by us and by others has proved that piperazine may connect two metal centers as a bridging ligand under basic conditions.[20] Inspired by this, we used basic conditions and the piperazinyl group as a ligand to synthesize extended metal–cfH complexes. Because the mixing of a metal salt and the cfH solution usually results in a precipitation, making it difficult to grow crystals of complexes, the hydrothermal technique was adopted in this paper to put the designed strategies into practice. This method afforded a series of new metal–cfH complexes: $[Ba_2(cf)_2(1,4\text{-bdc})(H_2O)_2]\cdot H_2O$ (**1**), $[Sr_6(cf)_6(1,4\text{-bdc})_3(H_2O)_6]\cdot 2H_2O$ (**2**), $[M_2(cfH)_2(bptc)(H_2O)_2]\cdot 8H_2O$ (M = Mn (**3**) and Cd (**4**)), [M(cfH)(1,3-bdc)] (M = Mn (**5**), Co (**6**), and Zn (**7**)), $[Zn_2(cfH)_4(1,4\text{-bdc})](1,4\text{-bdc})\cdot 13H_2O$ (**8**), $[Ca(cfH)_2(1,2\text{-Hbdc})_2]\cdot 2H_2O$ (**9**), and $[M(cf)_2]\cdot 2.5H_2O$ (M = Mn (**10**), Co (**11**), Zn (**12**), Cd (**13**), and Mg (**14**)). The syntheses and crystal structures of these compounds are reported here. This work may provide new insights into understanding the mechanisms of action of the quinolone antibacterial agents.

Results and Discussion

Description of the crystal structures: Single-crystal X-ray structural analysis of compound **1** shows that the structure is a unique two-dimensional (2D) arm-shaped layer containing one-dimensional Ba-O-Ba chains, in which the asymmetric unit contains 1 Ba atom, 1 cf ligand, 0.5 1,4-bdc ligand, 1 aqua ligand, and 0.5 free water molecule (Figure 1). The Ba atom is coordinated in a distorted triangle-dodecahedral geometry to three oxygen atoms from two chelating/bridging bis-bidentate 1,4-bdc ligands, to four oxygen atoms from

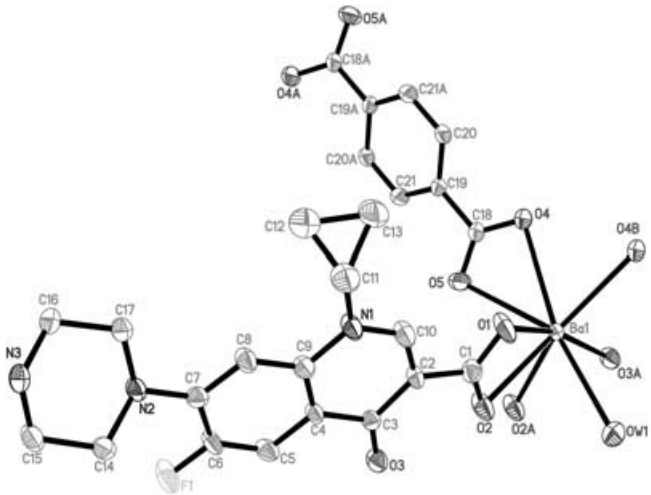

Figure 1. ORTEP diagram showing the coordination environment for the Ba atom in **1**.

two cf units, and to one aqua ligand. The Ba–O bond lengths are in the range of 2.637(2)–2.849(3) Å, and the O-Ba-O angles vary from 45.47(6) to 166.39(8)°. The carboxylic group of quinolone usually exhibits a monodentate coordination mode; however, in **1**, it acts as a chelating/bridging bidentate ligand to link two Ba centers. This coordination mode has not been observed in other metal-fluoroquinolone compounds (see Scheme S1 in the Supporting Information).[15,16]

The $\{BaO_8\}$ triangle-dodecahedrons are spontaneously connected in an edge-sharing mode to form a one-dimensional (1D) Ba-O-Ba chain along the *a* axis (Figure 2). The

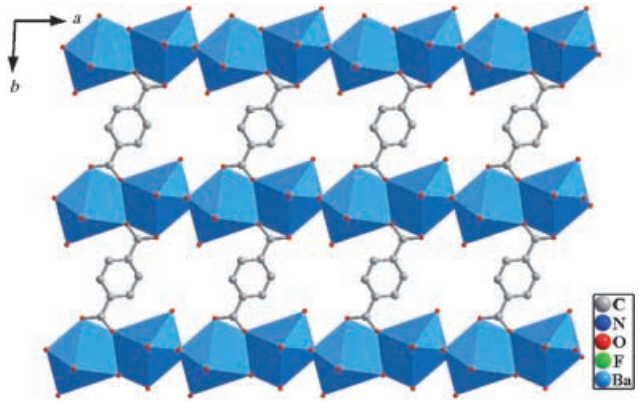

Figure 2. Perspective view of the 2D brick-wall network in **1**, showing parallelogrammic cavities with dimensions of 9.0×12.2 Å.

adjacent chains are further connected by the bridging 1,4-bdc ligands to produce an interesting 2D brick wall architecture with regular parallelogrammic cavities (9.0×12.2 Å based on $d_{Ba\cdots Ba}$). The cf groups, grafted on the 2D brick wall network, resemble open arms (with a length of ≈13.6 Å) that protrude from the both sides of the sheet (see Figure S1 in the Supporting Information). Under this premise, a nice example of interdigitation is generated. The adjacent layers in **1** are interdigitated in a zipper-like fashion to form a three-dimensional (3D) supramolecular framework (Figure 3) with significant hydrogen bonding interactions between the hydrogen atoms of the cf groups and the oxygen atoms of the sheets. The typical hydrogen bond lengths are C1–H1···O5 2.305 Å, C3–H3···O6 2.415 Å, and C21–H21···O4 2.562 Å.

When Ba is replaced by Sr, an alkaline earth metal of smaller radius, analogous 2D arm-shaped layers are formed in **2** under similar reaction conditions. The asymmetric unit of **2** has three crystallographically independent Sr atoms (Figure 4). The Sr1 and Sr2 centers adopt distorted triangular-dodecahedral geometries, being coordinated by three pairs of chelating oxygen atoms from one 1,4-bdc and two different cf ligands, respectively, one bridging oxygen atom from the carboxylic group of one 1,4-bdc unit, and one oxygen atom from the terminal water molecule. Whereas the Sr3 center is ligated by two pairs of chelating oxygen atoms from 1,4-bdc and cf ligands, two bridging oxygen

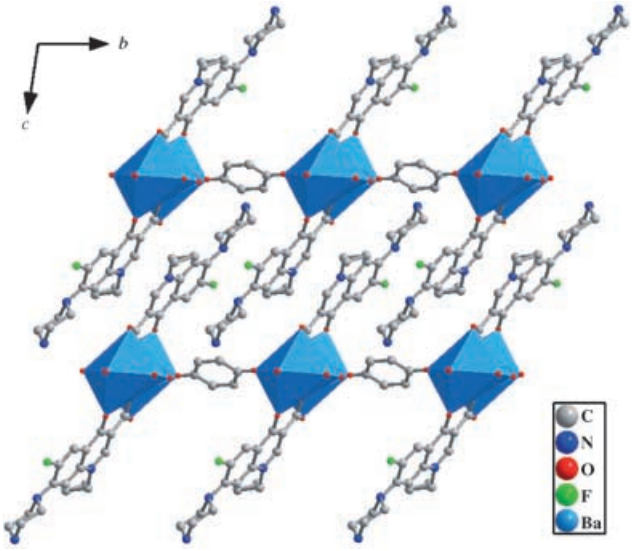

Figure 3. The packing arrangement of compound **1**, highlighting the interdigitation of the 2D arm-shaped layer.

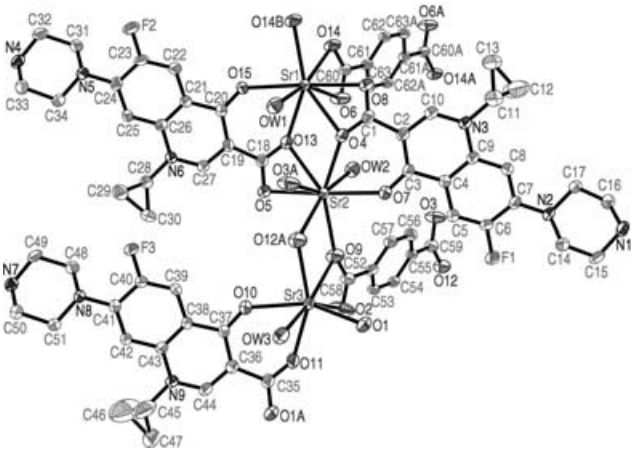

Figure 4. ORTEP diagram showing the coordination environments for Sr atoms in **2**.

atoms from the carboxylic groups of 1,4-bdc and cf ligands, and one aqua ligand to complete a distorted pentagonal-bipyramidal configuration. The Sr–O bond lengths are in the range of 2.490(3) –2.771(3) Å, and the O-Sr-O angles vary from 47.86(9) to 171.78(11)°. The three carboxylic groups of three crystallographically independent cf ligands exhibit two kinds of coordination modes with Sr centers. They are the chelating/bridging bidentate and bidentate mode, and, as far as we know, the latter coordination mode has not been observed in other metal–quinolone compounds (see Scheme S1 in the Supporting Information).[14]

The Sr1, Sr2, and Sr3 centers are connected by μ-oxygen atoms in an edge-sharing mode to form a new hexanuclear strontium cluster (Figure 5). Neighboring hexanuclear strontium clusters are linked by two carboxylic groups of the cf ligands to produce a 1D chain along the $[01\bar{1}]$ direction. Adjacent chains are further linked by the μ_6-1,4-bdc to generate

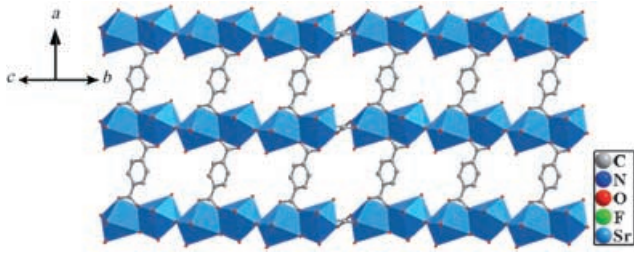

Figure 5. Perspective view of the 2D sheet in **2**, showing two types of parallelogrammic cavities with dimensions of 8.6×11.8 and 9.5×11.8 Å.

a 2D sheet (Figure 5). Interestingly, two types of regular parallelogrammic cavities (8.6×11.8 and 9.5×11.8 Å based on $d_{Sr\cdots Sr}$) coexist in the 2D sheet. Similar to compound **1**, the cf lateral arms (with a length of ≈13.5 Å), which are grafted on both sides of each sheet, penetrate into the parallelogrammic cavities of the adjacent sheets (Figure 6) thus result-

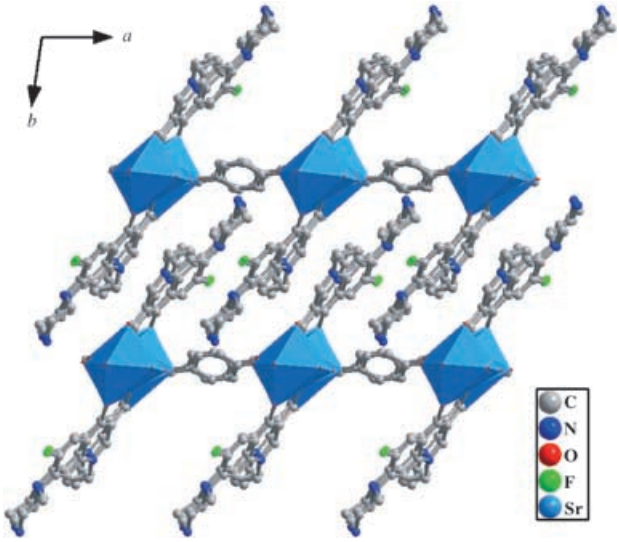

Figure 6. The packing arrangement of **2** viewed along the [01$\bar{1}$] direction, showing the interdigitation of 2D arm-shaped layer.

ing in a interdigitated 3D architecture. To date, there are still only a few examples of interdigitation with identical motifs.[21]

Compounds **3** and **4** are isostructural, hence only the structure of **4** will be discussed in detail. There are two unique Cd atoms in the asymmetric unit of **4** (Figure 7). Both Cd centers exhibit distorted octahedral geometries, and are coordinated to three oxygen atoms of two cf ligands, two oxygen atoms of one bptc ligand, and one aqua ligand. The Cd–O bond lengths are in the range of 2.216(3)-2.398(3) Å, and the O-Cd-O angles vary from 75.16(11) to 174.4(2)°. The coordination mode of the carboxylic groups of the cf ligands can be considered to be the monodentate bridging type (see Scheme S1 in the Supporting Information). On the basis of this connection mode, two {Cd(1)O_6} (or {Cd(2)O_6}) units are connected together by μ_3-O atoms of carboxylic groups from cf ligands in an edge-sharing

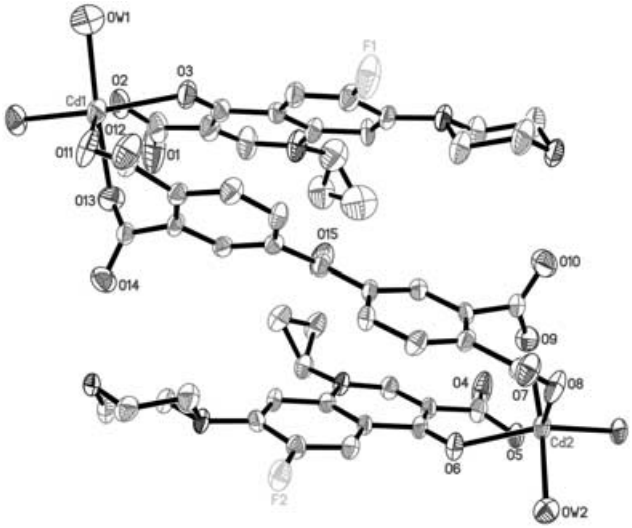

Figure 7. ORTEP diagram showing the coordination environments for Cd atoms in **4**.

mode to form [M_2(cfH)$_2$(H_2O)$_2$] dimers (Figure 8). To the best of our knowledge, such dimers have not been documented in the system of metal–cfH complexes.[15,16] Interest-

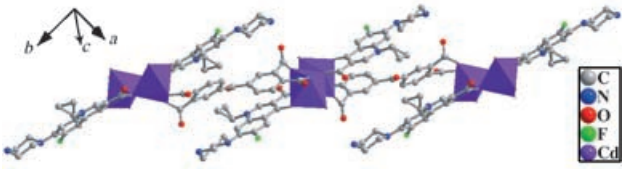

Figure 8. View of the 1D hybrid chain in **4**. Lattice water molecules have been omitted for clarity.

ingly, the dimers are further connected by a bptc ligand through four monodentate carboxylic groups to generate a distinct 1D chain (Figure 8). It is worth mentioning here that the coordination chemistry of bptc has not been previously investigated. In the packing arrangement of **4**, the adjacent 1D chains are interdigitated in a zipper-like fashion to form undulating 2D layers with significant hydrogen bonding interactions between the hydrogen atoms of the piperazinyl groups and the carboxyl oxygen atoms (N4···O10 2.750 Å, N4···O9 3.297 Å, and C33···O5 3.481 Å) (Figure S2). These layers are further connected by means of N–H···O and C–H···O hydrogen bonds (N1···O7 2.724 Å, C15···O4 3.279 Å, C15···O8 3.048 Å, and C32···O7 3.204 Å) to generate a 3D network featuring large cavities with dimensions of 11.2×8.8×14.0 Å. As shown in Figure 9, these cavities are connected to each other with a small window of approximately 3.8 Å to from a 1D zigzag channel along the *b* axis. Free water molecules are located in the channels and form multipoint hydrogen bonds with coordinated water molecules and carboxyl oxygen atoms.

When 1,3-bdc was used instead of bptc, structurally different 1D chains were formed in **5**, **6**, and **7**. Compounds **5**, **6**,

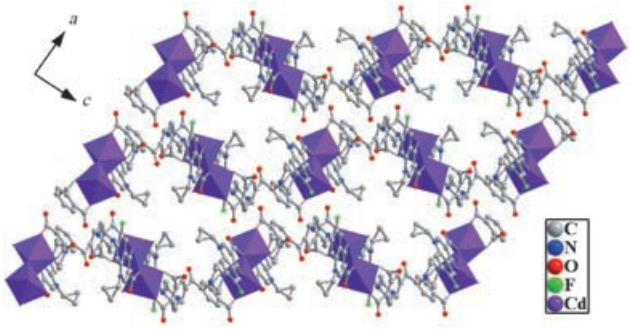

Figure 9. Perspective view of the 3D supramolecular network in **4**, highlighting the zigzag channels along the *b* axis. Guest water molecules included in the channels are omitted for clarity.

and **7** are isostructural, so only the structure of **5** is discussed herein. The asymmetric unit of **5** consists of one manganese atom, one 1,3-bdc ligand, and one coordinated cfH molecule (Figure 10). Each Mn^{II} center displays a distorted octahedral coordination geometry, and is coordinated to two oxygen

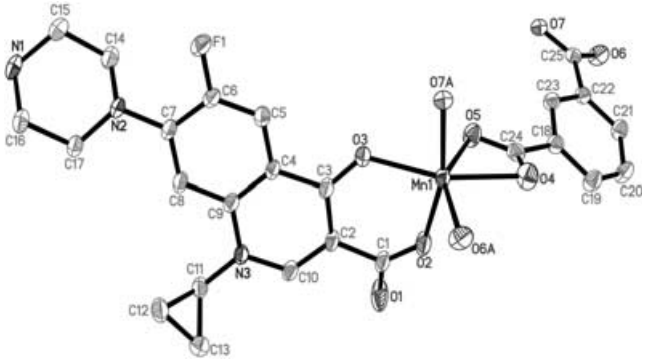

Figure 10. ORTEP diagram showing the coordination environment for Mn atoms in **5**.

atoms of one cf ligand and four oxygen atoms from three different carboxylic groups of three 1,3-bdc ligands. The average Mn–O bond length is 2.1991 Å, in good agreement with previous studies.[22] The 1,3-bdc ligand exhibits an interesting connection mode to the Mn^{II} atom: two carboxylic groups display two different kinds of coordination modes, that is, the chelating bidentate and bidentate mode. Based on these connection modes, two Mn^{II} ions are bridged by a pair of the 1,3-bdc μ-carboxylate ends into a dimer unit (Figure 11). Such a $[M_2(cfH)_2(CO_2)_2]$ dimer has not been reported in the system of metal-quinolones.[14] It is interesting that every two dimers are further linked by two 1,3-bdc ligands along two different alternating directions to form a double-chain-like ribbon (Figure 11). The adjacent ribbons are packed through interdigitation of the lateral cf ligands (N1···O1 2.651 Å) in a zipper-like fashion into 2D networks (see Figure S4 in the Supporting Information), which are further extended by N–H···O and C-H···O hydrogen bonds (N1···O5 2.813 Å and C16···O7 3.383 Å) into a 3D supramolecular architecture (Figure 12).

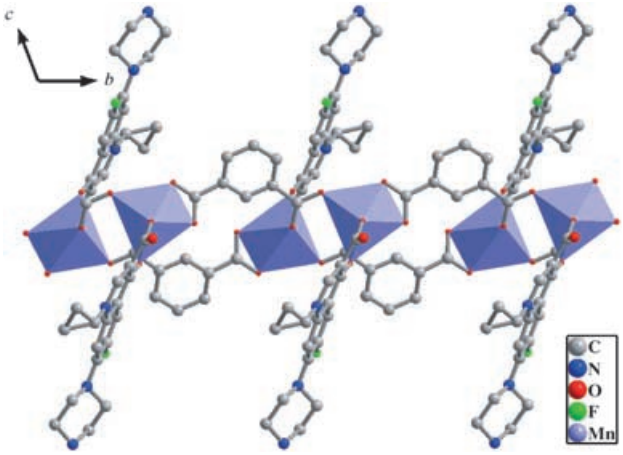

Figure 11. View of the 1D double-chain-like ribbon in **5**.

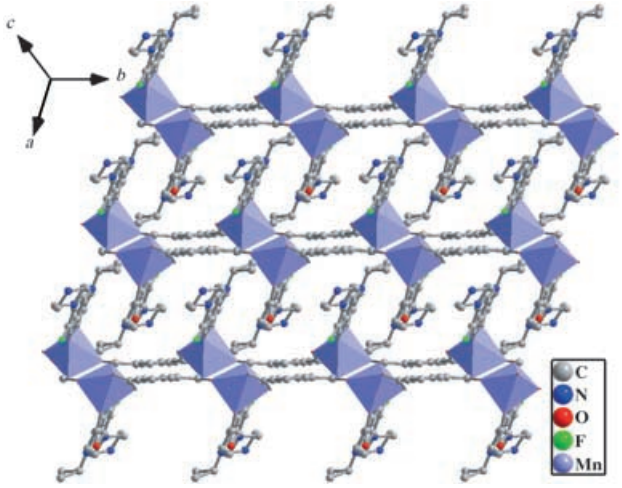

Figure 12. The packing arrangement of compound **5**, viewed along the [111] direction.

The structure of **8** consists of a pair of $[Zn(cfH)_2]^{2+}$ fragments bridged by a deprotonated 1,4-bdc into a dinuclear dumbbell-shaped molecule (Figure 13). The crystallographically unique Zn^{II} is in the center of a distorted octahedron, which is defined by four oxygen atoms of two different cf ligands and two oxygen atoms from one chelating bis-bidentate 1,4-bdc ligand. The Zn–O bond lengths are in the range of 2.014(4)-2.208(4) Å, and the O-Zn-O angles vary from 58.9(2) to 176.6(2)°. There are two types of supramolecular interactions in **8**, namely hydrogen bonding and aromatic π–π stacking interactions. First, the cf ligands between adjacent dumbbell-shaped molecules are arranged in an offset fashion with a plane-to-plane separation of 3.2–3.3 Å, indicating strong aromatic π–π stacking interactions. Thus, discrete molecules of **8** are extended into 2D supramolecular arrays (see Figure S6 in the Supporting Information). Second, the N–H···O and C–H···O hydrogen bonds (N3···O2 2.746 Å and C16···O1 3.193 Å) further extend the 2D supramolecular arrays into an interesting 3D supramolecular network featuring multidirectional intersecting cationic channels

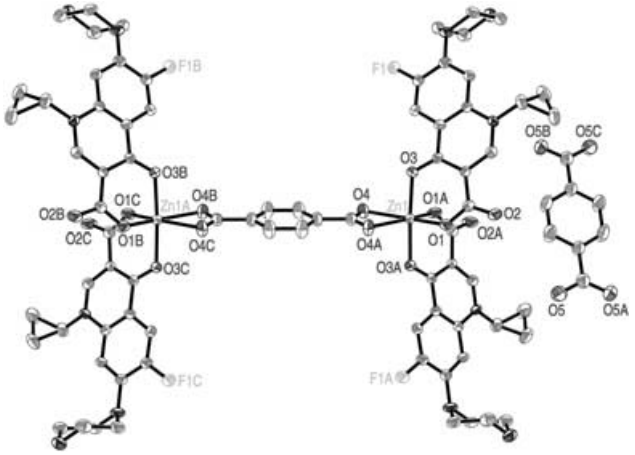

Figure 13. ORTEP drawing of **8** with thermal ellipsoids at 50% probability. The lattice water molecules have been omitted for clarity.

(Figure 14, and Figure S7a–c in the Supporting Information). Completely deprotonated 1,4-bdc guests and free water molecules reside in the channels. There is also extensive hydrogen-bonding interactions among water molecules, 1,4-bdc, and dumbbell-shaped dimers. Therefore, the architecture of **8** can be best described as a 3D supramolecular host–guest network.

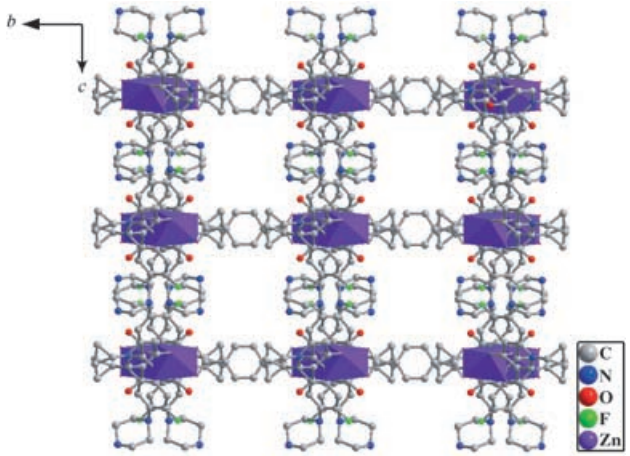

Figure 14. Perspective view of the 3D supramolecular network in **8**, highlighting the rectangular channels along the *a* axis. Free organic molecules and water molecules included in the channels are omitted for clarity.

X-ray crystallographic analysis reveals that the structure of compound **9** consists of a neutral mononuclear $[Ca(cfH)_2(1,2\text{-}Hbdc)_2]$ complex and two water molecules linked by a hydrogen-bonding network. Each Ca^{II} atom in **9** is coordinated to four oxygen atoms from two cf ligands in the equatorial positions while two oxygen atoms of two 1,2-bdc ligands occupy the axial positions resulting in a distorted octahedral geometry (Figure 15). The Ca–O bond lengths are in the range of 2.2860–2.3203 Å, and the O-Ca-O angles vary from 75.12 to 180.00°. The supramolecular structure of **9** is mainly stabilized by hydrogen bonding and aromatic π–

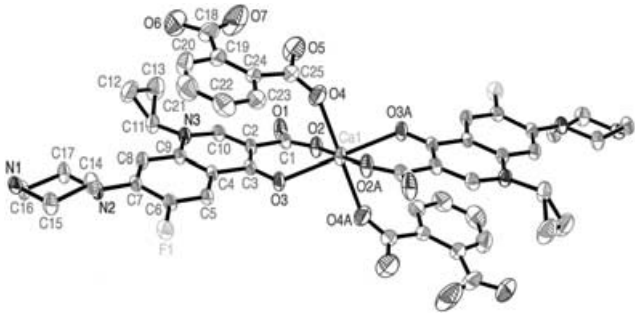

Figure 15. ORTEP drawing of **9** with thermal ellipsoids at 50% probability. The lattice water molecules have been omitted for clarity.

π stacking interactions. The N-H···O, OW-H···O, and C-H···O hydrogen bonds (N1···O1 2.724, N1···O2 3.179, N1···O6 2.709, OW1···O3 3.001, OW1···O5 3.162, C16···O2 3.458, and C11···OW1 3.344 Å) link the discrete molecules into 2D arrays (see Figure S8a in the Supporting Information). These 2D layers are further extended through off-set aromatic π–π stacking interactions of cf groups (separation 3.4–3.5 Å) into the final 3D supramolecular arrays (Figure S8c). It is worth noting that the metal-quinolone complexes containing alkaline-earth metal elements are particularly rare,[14] although alkaline-earth metal ions are very important in biology. As far as we know, compounds **1**, **2**, **9**, and **14** represent the first members of s series of structurally characterized metal–cfH complexes containing alkaline-earth metal ions.

In a comparison of the structures of **1**–**9**, it was found that the coordination modes of the polycarboxylate ligands and the coordination geometry of the central metal ion may have a very significant effect on the formation and dimension of the resulting structure. As demonstrated by a comparison of compounds **1** and **2** with **8**, the high coordination number of the metal is a critical factor for the formation of a high-dimensional structure. In addition, the steric geometry of the polycarboxylate ligands also plays a crucial role in the construction of extended metal–cfH complexes. Owing to the steric hindrance of the bulky cf ligands, the distance between the carboxylic groups and the length of the polycarboxylate ligands are essential for the generation of the extended structure, as evidenced by the comparison of compounds **3**–**7** with **9**. Furthermore, by inspection of the structures of **1**–**7**, we believed that the formation of polynuclear metal SBUs plays an important role in stabilizing the polymeric extended structure.

Interestingly, when the hydrothermal reactions of cfH and the metal salt were carried out at a pH of approximately 11–12, a series of 2D complexes $[M(cf)_2]\cdot 2.5H_2O$ (M = Mn(**10**), Co(**11**), Zn(**12**), Cd(**13**), and Mg(**14**)) were isolated. Complexes **10**–**14** are isostructural, and the structure of **10** will be discussed in detail as an example. In the crystal structure of **10**, each independent crystallographic unit contains 0.5 Mn^{II} atom, 1 cf ligand, and 1.25 lattice water molecules (Figure 16). Each Mn^{II} is ligated by four oxygen atoms (Mn–O 2.1449(16) and 2.1562(13) Å) from carbonyl and carboxyl

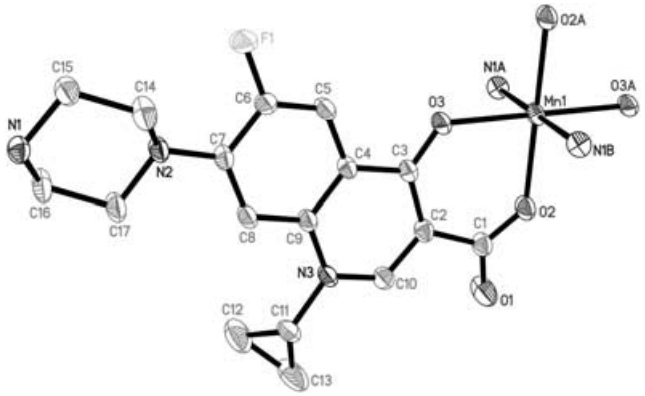

Figure 16. ORTEP drawing of **10** with thermal ellipsoids at 50% probability. The lattice water molecules have been omitted for clarity.

groups of two different cf ligands at equatorial positions, and by two nitrogen atom from piperazinyl groups of two cf ligands (Mn–N 2.3465(15) Å) at the apical positions to furnish a distorted octahedral geometry. Because the terminal nitrogen atom of the piperazine is also involved in the binding to the metal, the cf ligand acts as a bridging ligand to link two metal centers. To our knowledge, this is the first time that this coordination mode has been observed in metal–cfH complexes.[15,16] On the basis of this connection mode, all the Mn centers are linked by four bridging cf ligands to generate a 2D rhombic grid featuring large cavities with dimensions of 13.6×13.6 Å (Figure 17 and Figure S9 in

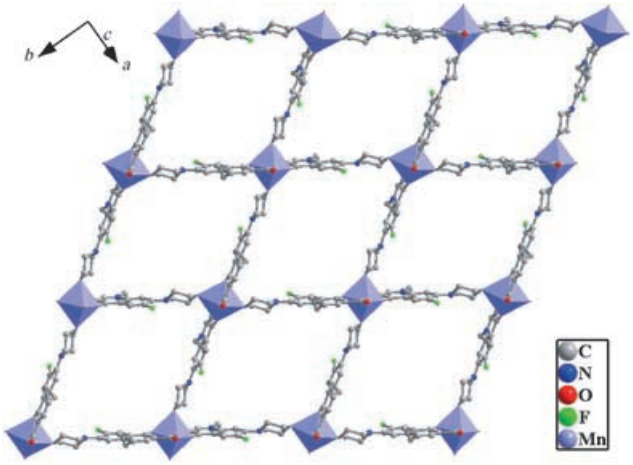

Figure 17. A view of the two-dimensional grid sheet in **10**, highlighting regular rhombic cavities with dimensions of 13.6×13.6 Å.

the Supporting Information). These layers display a short interlayer separation of 5.9 Å, and the cf ligands of adjacent grids interact with each other through hydrogen bonding (N1···O1 3.215, N1···O2 3.290, C11···N2 3.551, and C14···O1 3.277 Å) and aromatic π–π stacking (separation 3.3–3.4 Å) interactions. Thus, the adjacent 2D grids are perfectly overlapped together to generate nanosized channels along the [100] direction (Figure 18). Free water molecules, located in the channels, form hydrogen-bonding interactions with un-

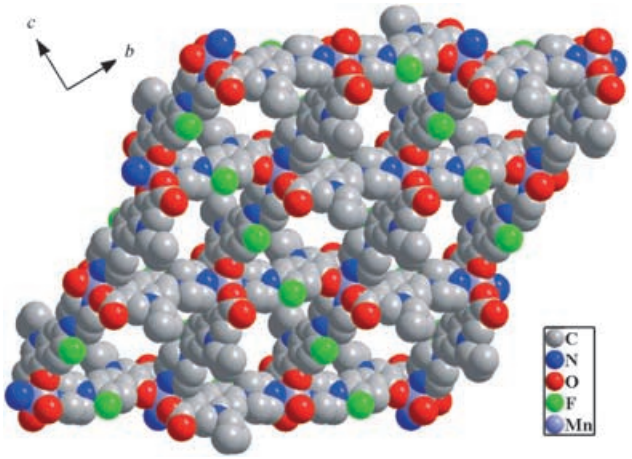

Figure 18. Space-filling diagram of the 3D supramolecular structure of **10**, showing the nanosized channels along the [100] direction. Guest water molecules included in the channels are omitted for clarity.

coordinated oxygen atoms from the carboxylic groups of the cf ligands (OW1···O1 2.744 Å; OW2···O1 2.911 Å). It is worth mentioning here that the nanosized neutral 2D grid is non-interpenetrated, which is particularly rare and appears to be very useful for host–guest chemistry.

The profound influence of the pH on the final structure is revealed in the comparison of compounds **10**–**14** with **3**–**9**. The cfH molecules can exist in four possible forms: an acidic cation cfH_2, a neutral non-ionized species cfH, an intermediate zwitterion cfH^{+-}, and a basic anion cf^-, depending on the pH. At low pH values, both the piperazinyl group and the carboxyl group are protonated, whereas at high pH values, neither is protonated. Thus, the coordination of cfH to the metal ions also depends on the pH of the solution. In a basic solution, the N atom of the piperazinyl group can take part in the coordination to the metal ion, while the N atom of the piperazinyl group is protonated in a weak acidic solution and thus fails to bind to the metal ion. It is of great interest to investigate the effect of pH in metal–cfH systems because it helps us to understand the correlation between the reaction acidity and the resulting structure. This thus leads to the possibility of predicting the structure of the metal–cfH complex obtained.

Photoluminescence properties: The solid-state emission spectra of compounds **7**, **8**, **12**, and **13** at room temperature are depicted in Figure 19. It can be observed that intense emissions occur at 421 nm (Figure 19a, λ_{ex} = 382 nm) for **7**, 420 nm (Figure 19b, λ_{ex} = 370 nm) for **8**, 419 nm (Figure 19c, λ_{ex} = 372 nm) for **12**, and 430 nm (Figure 19d, 398 nm) for **13**. To understand the nature of the emission band, the photoluminescence property of cfH ligand was analyzed. A similar weak emission (λ_{max} = 431 nm) was observed for the free cfH ligand (see Figure S17 in the Supporting Information). Therefore, the emissions of **7**, **8**, **12**, and **13** may be assigned to intraligand fluorescent emission. The enhancement of luminescence may be attributed to ligand chelation to the metal center, which effectively in-

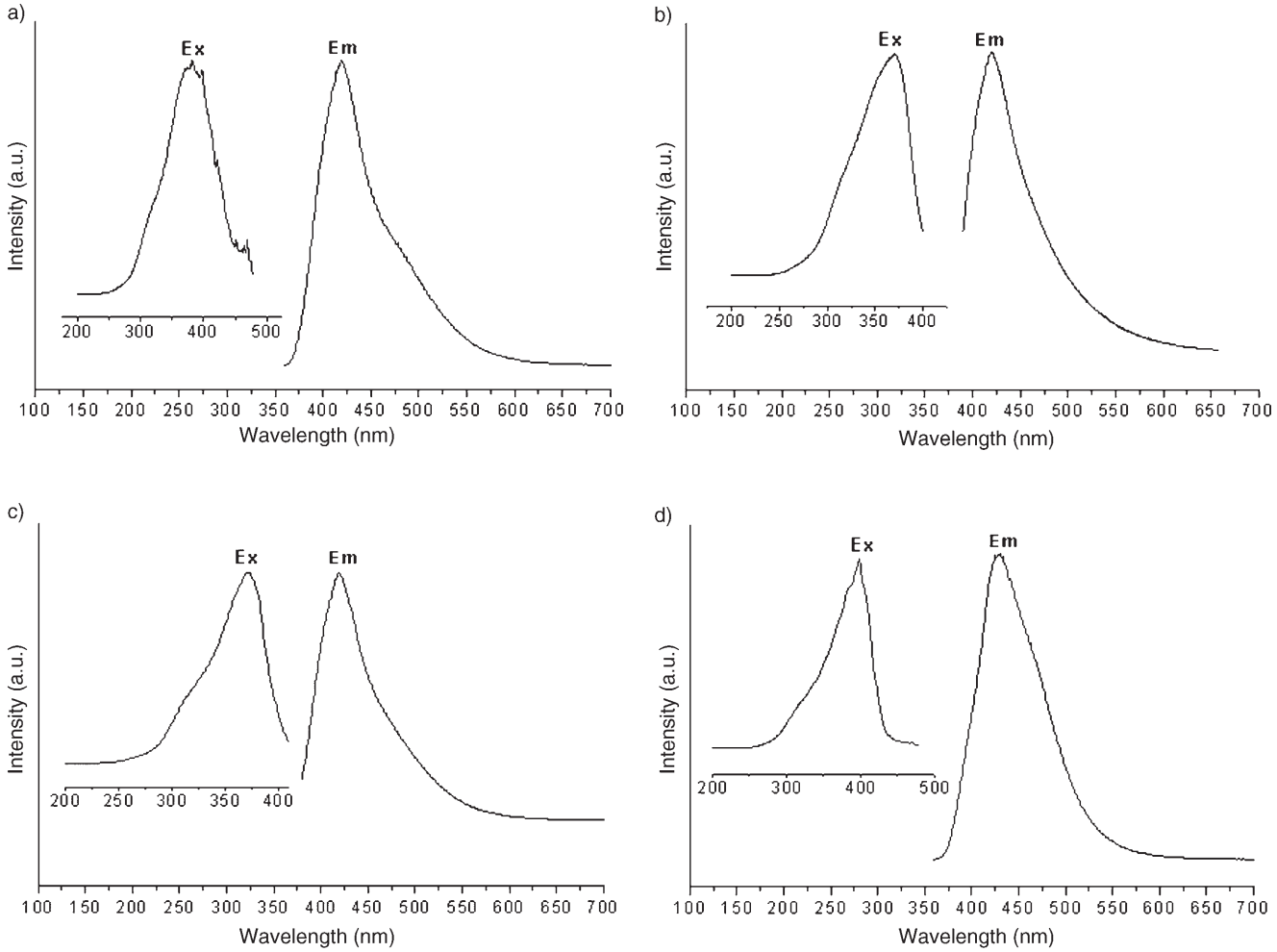

Figure 19. Solid-state emission spectra of complexes at room temperature: a) **7**, b) **8**, c) **12**, d) **13**.

creases the rigidity of the ligand and reduces the loss of energy by radiationless decay. These observations indicate that compounds **7**, **8**, **12**, and **13** may be excellent candidates for potential photoactive materials because these condensed materials are thermally stable and insoluble in common polar and nonpolar solvents.

Magnetic properties: The magnetic properties of **3**, **5**, **10**, and **11** were investigated over the temperature range 2.0–300.0 K (Figure 20). For **3**, the $\chi_M T$ value at 300 K is 7.747 $cm^3 K mol^{-1}$ (7.872 μ_B), smaller than the expected value (8.750 $cm^3 K mol^{-1}$, 8.367 μ_B) of two isolated spin-only Mn^{II} ions ($S = {}^5/_2$, $g = 2.0$; Figure 20a). $\chi_M T$ gradually increases as the temperature is lowed and reaches a maximum value of 8.432 $cm^3 K mol^{-1}$ at 55 K, and then decreases to 5.215 $cm^3 K mol^{-1}$ at 2 K. The high-temperature regime is typically observed for paramagnetic systems that exhibit dominating ferromagnetic interactions, while the $\chi_M T$ decrease at low temperature is usually the signature of a weak antiferromagnetic interaction between Mn^{II} metal ions and/or a zero-field splitting (ZFS) effect. Based on the structure analysis of **3**, the ferromagnetic interaction between Mn centers is expected to be through the Mn···Mn dinuclear units (the distance of Mn···Mn is 3.495 Å), while bptc bridges will lead to weaker antiferromagnetic interactions. The $1/\chi_M$ versus T plot of **3** is in correspondence with Curie–Weiss law in the range of 2–300 K with $C = 7.867\ cm^3 K mol^{-1}$ and $\theta = 2.356$ K.

For **5**, the $\chi_M T$ value at 300 K is 3.658 $cm^3 K mol^{-1}$ (5.409 μ_B), which is slightly smaller than the expected value (4.375 $cm^3 K mol^{-1}$, 5.916 μ_B) of one isolated spin-only Mn^{II} ion ($S = {}^5/_2$, $g = 2.0$; Figure 20b). The $\chi_M T$ value of **5** remains almost constant from 300 K to 110 K, and then decreases on further cooling, reaching a value of 0.351 $cm^3 K mol^{-1}$ at 2 K. This behavior indicates a dominant antiferromagnetic interaction between the Mn^{II} ions in the structures. Based on the structure analysis of **5**, the antiferromagnetic interaction between Mn centers is expected to be through the carboxylate bridge. The fit of the curve for $1/\chi_M$ versus T plot of **5** to the Curie–Weiss law gives a good result in the temperature range of 8–300 K with $C = 3.877\ cm^3 K mol^{-1}$ and $\theta = -7.987$ K.

For **10**, the $\chi_M T$ value at 300 K is 4.576 $cm^3 K mol^{-1}$ (6.050 μ_B), which is slightly higher than the expected value

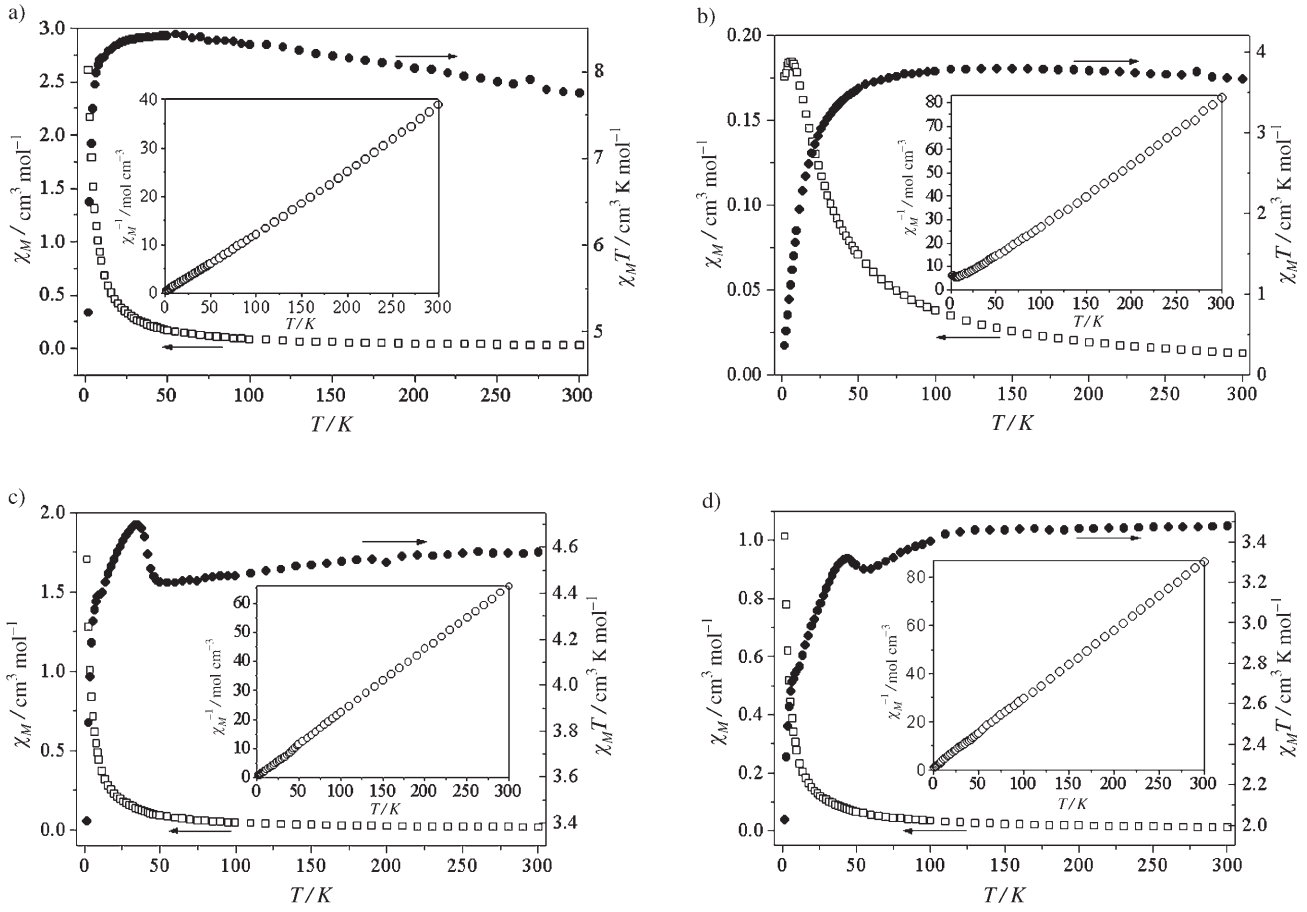

Figure 20. Thermal variation of χ_M and $\chi_M T$ of the compound. Insert: plot of the thermal variation of χ_M^{-1} for the respective compound. a) **3**, b) **5**, c) **10**, d) **11**.

(4.375 cm^3 K mol^{-1}, 5.916 μ_B) of one isolated spin-only Mn^{II} ion ($S = {}^5/_2$, $g = 2.0$; Figure 20c). As T is lowered, $\chi_M T$ continuously decreases to a value of 4.444 cm^3 K mol^{-1} at 53 K, and then increases to a maximum of 4.696 cm^3 K mol^{-1} at 34 K. Below this temperature, $\chi_M T$ decreases sharply and reaches 3.406 cm^3 K mol^{-1} at 2 K. For **11**, the $\chi_M T$ value at 300 K is 3.475 cm^3 K mol^{-1} (5.273 μ_B), which is much higher than the expected value (1.875 cm^3 K mol^{-1}, 3.873 μ_B) of one isolated spin-only Co^{II} ion ($S = {}^3/_2$, $g = 2.0$; Figure 20d). As T is lowered, $\chi_M T$ continuously decreases and reaches a local minimum of 3.262 cm^3 K mol^{-1} at 55 K, and then increases to a value 3.317 cm^3 K mol^{-1} at 44 K, before dropping quickly to 2.025 cm^3 K mol^{-1} at 2 K. The magnetic behaviors of **10** and **11** are unusual and interesting, indicative of a strong antiferromagnetic interaction admixture with a very weak ferromagnetic interaction.[23] Fits of the curve for $1/\chi_M$ versus T plots of **10** and **11** to the Curie–Weiss law give good results in the temperature range of 2–300 K with C = 4.568 cm^3 K mol^{-1} and $\theta = -0.617$ K for **10**, and C = 3.510 cm^3 K mol^{-1} and $\theta = -2.961$ K for **11**.

Conclusion

In summary, two rational synthetic strategies were developed to successfully produce a series of polymeric extended metal–cfH complexes. One is based on introducing aromatic polycarboxylate ligands into the reaction system and the other directly utilizes cf as a bridging ligand under basic reaction conditions. The successful isolation of the solids **1**–**14** provides not only the first examples of extended metal–cfH complexes, but also new structural information that will aid in understanding the mechanisms of action of the quinolone antibacterial drugs. The new design idea depicted in this paper may be a promising technique for the construction of many other metal-quinolone complexes with polymeric extended structures, thus opening a new avenue in the exploration of extended metal-quinolone complexes.

Experimental Section

Materials and physical measurements: All chemicals were commercially purchased and used without further purification. Elemental analyses (C, H, and N) were performed on a Perkin-Elmer 2400 CHN Elemental Analyzer. Ba, Sr, Mn, Cd, Co, Zn, Ca, and Mg were determined by a Leaman

inductively-coupled plasma (ICP) spectrometer. IR spectra were recorded in the range 400–4000 cm^{-1} on an Alpha Centaurt FT/IR Spectrophotometer as KBr pellets. TG analyses were performed on a Perkin-Elmer TGA7 instrument in flowing N_2 with a heating rate of 10 °C min^{-1}. Excitation and emission spectra were obtained on a SPEX FL-2T2 spectrofluorometer equipped with a 450 W xenon lamp as the excitation source. Variable-temperature magnetic susceptibility data were obtained on a SQUID magnetometer (Quantum Design, MPMS-7) at 2–300 K with an applied field of 10 KG.

$[Ba_2(cf)_2(1,4\text{-}bdc)(H_2O)_2]\cdot H_2O$ (1): A mixture of $BaCl_2\cdot 2H_2O$ (0.5 mmol), ciprofloxacin hydrochloride (0.5 mmol), 1,4-H_2bdc (0.25 mmol), NaOH (0.5 mmol), and water (7 mL) was stirred for 30 min in air (solution pH 7.0). The mixture was transferred and sealed into an 18-mL Teflon-lined autoclave, which was heated at 120 °C for 89 h. After the mixture had been allowed to slowly cool to room temperature, colorless blocks of **1** were filtered off, washed with distilled water, and dried at ambient temperature (yield: 70% based on Ba). IR (KBr): $\tilde{\nu}$ = 3519 (br), 3378 (w), 3308 (m), 2852 (w), 1618 (s), 1579 (s), 1556 (s), 1489 (m), 1478 (m), 1457 (m), 1388 (s), 1324 (m), 1298 (s), 1257 (s), 1250 (s), 1178 (m), 1134 (m), 1118 (m), 1042 (m), 928 (m), 881 (m), 864 (w), 839 (m), 824 (m), 783 (w), 757 (m), 739 (m), 713 (w), 625 (m), 550 (w), 496 (m) cm^{-1}; elemental analysis calcd (%) for $C_{42}H_{44}Ba_2F_2N_6O_{13}$: C 43.73, H 3.84, Ba 23.81, N 7.29; found: C 43.61, H 3.90, Ba 23.88, N 7.23.

$[Sr_6(cf)_6(1,4\text{-}bdc)_3(H_2O)_6]\cdot 2H_2O$ (2): Compound **2** was prepared as for **1** with $SrCl_2\cdot 6H_2O$ instead of $BaCl_2\cdot 2H_2O$. Colorless blocks of **2** were obtained in a 75% yield. IR (KBr): $\tilde{\nu}$ = 3509 (br), 3358 (w), 3314 (w), 2852 (w), 1623 (s), 1582 (s), 1560 (s), 1479 (m), 1458 (m), 1398 (s), 1324 (m), 1299 (s), 1251 (s), 1178 (m), 1134 (m), 1119 (m), 1043 (m), 1021 (m), 951 (m), 930 (m), 881 (m), 864 (m), 837 (w), 824 (s), 783 (w), 757 (m), 744 (m), 713 (w), 627 (m), 550 (w), 499 (m) cm^{-1}; elemental analysis calcd (%) for $C_{126}H_{130}F_6N_{18}O_{38}Sr_6$: C 48.13, H 4.17, N 8.02, Sr 16.72; found: C 48.21, H 4.11, N 8.08, Sr 16.65.

$[Mn_2(cfH)_2(bptc)(H_2O)_2]\cdot 8H_2O$ (3): A mixture of $Mn(OAc)_2\cdot 4H_2O$ (0.5 mmol), ciprofloxacin hydrochloride (0.5 mmol), H_4bptc (0.25 mmol), and water (7 mL) was stirred for 30 min in air (solution pH 4.0). The mixture was transferred and sealed into an 18-mL Teflon-lined autoclave, which was heated at 110 °C for 96 h. After the mixture had been allowed to slowly cool to the room temperature, yellow blocks of **3** were filtered off, washed with distilled water, and dried at ambient temperature (yield: 78% based on Mn). IR (KBr): $\tilde{\nu}$ = 3391 (br m), 2845 (w), 1629 (s), 1567 (s), 1486 (s), 1456 (m), 1424 (m), 1382 (s), 1331 (m), 1274 (s), 1247 (m), 1181 (m), 1141 (m), 1109 (w), 1083 (w), 1027 (m), 1005 (w), 943 (m), 896 (w), 848 (m), 835 (s), 819 (m), 785 (w), 751 (m), 665 (m), 627 (m), 544 (w), 498 (w) cm^{-1}; elemental analysis calcd (%) for $C_{51}H_{62}F_2Mn_2N_6O_{25}$: C 46.87, H 4.78, Mn 8.41, N 6.43; found: C 46.78, H 4.83, Mn 8.47, N 6.49.

$[Cd_2(cfH)_2(bptc)(H_2O)_2]\cdot 8H_2O$ (4): The preparation of **4** was similar to that of **3** except that $Cd(NO_3)_2\cdot 4H_2O$ was used instead of $Mn(OAc)_2\cdot 4H_2O$. Colorless blocks were obtained in 80% yield. IR (KBr): $\tilde{\nu}$ = 3409 (br m), 2844 (w), 1626 (s), 1567 (s), 1486 (s), 1456 (m), 1382 (s), 1333 (m), 1272 (s), 1244 (m), 1181 (m), 1142 (m), 1108 (w), 1083 (w), 1026 (m), 1005 (w), 943 (m), 896 (w), 848 (m), 833 (m), 817 (m), 786 (w), 748 (m), 665 (m), 627 (m), 543 (w), 501 (w) cm^{-1}; elemental analysis calcd (%) for $C_{51}H_{62}Cd_2F_2N_6O_{25}$: C 43.08, H 4.39, Cd 15.81, N 5.91; found: C 43.15, H 4.44, Cd 15.73, N 5.85.

[Mn(cfH)(1,3-bdc)] (5): A mixture of $Mn(OAc)_2\cdot 4H_2O$ (0.5 mmol), ciprofloxacin hydrochloride (0.5 mmol), 1,3-H_2bdc (0.5 mmol), and water (7 mL) was stirred for 30 min in air (solution pH 4.0). The mixture was transferred and sealed into an 18-mL Teflon-lined autoclave, which was heated at 110 °C for 96 h. After the mixture was allowed to slowly cool to room temperature, yellow platelets of **5** were filtered off, washed with distilled water, and dried at ambient temperature (yield: 81% based on Mn). IR (KBr): $\tilde{\nu}$ = 3065 (w), 2988 (w), 2957 (w), 2851 (w), 1630 (s), 1615 (s), 1556 (s), 1531 (m), 1482 (s), 1454 (m), 1437 (m), 1382 (s), 1336 (m), 1300 (s), 1267 (m), 1253 (m), 1185 (m), 1159 (m), 1145 (w), 1128 (w), 1107 (w), 1093 (w), 1072 (w), 1049 (m), 1026 (m), 979 (m), 942 (m), 916 (m), 896 (m), 858 (m), 828 (m), 819 (m), 783 (w), 762 (s), 738 (s), 719 (s), 659 (m), 626 (m), 571 (m), 551 (m), 542 (m), 507 (m), 486 (m), 455 (m), 416 (m) cm^{-1}; elemental analysis calcd (%) for $C_{25}H_{22}FMnN_3O_7$: C 54.56, H 4.03, Mn 9.98, N 7.63; found: C 54.49, H 4.08, Mn 9.92, N 7.68.

[Co(cfH)(1,3-bdc)] (6): The preparation of **6** was similar to that of **5** except that $Co(OAc)_2\cdot 4H_2O$ was used instead of $Mn(OAc)_2\cdot 4H_2O$. Purple platelet crystals of **6** were obtained in 79% yield.; IR (KBr): $\tilde{\nu}$ = 3065 (w), 2988 (w), 2957 (w), 2851 (w), 1635 (s), 1614 (s), 1570 (s), 1532 (m), 1483 (s), 1456 (m), 1435 (m), 1382 (s), 1337 (m), 1301 (s), 1268 (m), 1254 (m), 1186 (m), 1159 (m), 1146 (w), 1107 (w), 1093 (w), 1071 (w), 1049 (m), 1028 (m), 980 (m), 943 (m), 923 (w), 895 (m), 859 (m), 826 (m), 818 (m), 786 (w), 762 (s), 742 (s), 719 (s), 659 (m), 628 (m), 574 (m), 554 (m), 544 (m), 507 (w), 486 (w), 455 (w), 419 (m) cm^{-1}; elemental analysis calcd (%) for $C_{25}H_{22}CoFN_3O_7$: C 54.16, H 4.00, Co 10.63, N 7.58; found: C 54.08, H 4.04, Co 10.69, N 7.53.

[Zn(cfH)(1,3-bdc)] (7): The preparation of **7** was similar to that of **5** except that $Zn(OAc)_2\cdot 2H_2O$ was used instead of $Mn(OAc)_2\cdot 4H_2O$. Colorless block crystals of **7** were obtained in 70% yield. IR (KBr): $\tilde{\nu}$ = 3071 (w), 2988 (w), 2957 (w), 2850 (w), 1615 (s), 1558 (s), 1530 (m), 1483 (s), 1455 (m), 1441 (m), 1357 (m), 1337 (m), 1301 (s), 1268 (s), 1253 (m), 1186 (m), 1160 (m), 1145 (w), 1129 (w), 1108 (w), 1095 (w), 1070 (w), 1048 (m), 1028 (m), 982 (m), 943 (s), 923 (m), 895 (m), 859 (m), 830 (m), 818 (m), 783 (w), 762 (s), 740 (s), 723 (s), 658 (m), 627 (m), 574 (m), 553 (m), 543 (m), 508 (m), 488 (m), 456 (m), 419 (m) cm^{-1}; elemental analysis calcd (%) for $C_{25}H_{22}FN_3O_7Zn$: C 53.54, H 3.95, N 7.49, Zn 11.66; found: C 53.43, H 3.90, N 7.41, Zn 11.78.

$[Zn_2(cfH)_4(1,4\text{-}bdc)](1,4\text{-}bdc)\cdot 13H_2O$ (8): A mixture of $Zn(OAc)_2\cdot 2H_2O$ (0.5 mmol), ciprofloxacin hydrochloride (0.5 mmol), 1,4-H_2bdc (0.5 mmol), and water (7 mL) was stirred for 30 min in air(solution pH 4.0). The mixture was transferred and sealed into an 18 mL Teflon-lined autoclave, which was heated at 110 °C for 96 h. After the mixture had been allowed to slowly cool to room temperature, yellow blocks of **8** were filtered off, washed with distilled water, and dried at ambient temperature (yield: 39% based on Zn). IR (KBr): $\tilde{\nu}$ = 3427 (br m), 3008 (w), 2841 (w), 2741 (w), 1628 (s), 1566 (s), 1485 (s), 1366 (s), 1305 (s), 1266 (s), 1182 (w), 1146 (w), 1105 (w), 1031 (m), 943 (m), 895 (m), 863 (w), 838 (m), 817 (m), 792 (w), 752 (s), 708 (w), 628 (w), 579 (m), 548 (m), 504 (m), 442 (w) cm^{-1}; elemental analysis calcd (%) for $C_{84}H_{106}F_4N_{12}O_{33}Zn_2$: C 49.98, H 5.29, N 8.33, Zn 6.48; found: C 49.87, H 5.33, N 8.39, Zn 6.56.

$[Ca(cfH)_2(1,2\text{-}Hbdc)_2]\cdot 2H_2O$ (9): A mixture of $CaCl_2$ (0.25 mmol), ciprofloxacin hydrochloride (0.5 mmol), 1,2-KHbdc (0.5 mmol), and water (7 mL) was stirred for 30 min in air (solution pH 4.0). The mixture was transferred and sealed into an 18-mL Teflon-lined autoclave, which was heated at 110 °C for 96 h. After the mixture had been allowed to slowly cool to room temperature, colorless blocks of **9** were filtered off, washed with distilled water, and dried at ambient temperature (yield: 67% based on Ca). IR (KBr): $\tilde{\nu}$ = 3505 (br), 3013 (w), 2855 (m), 2771 (w), 1631 (s), 1615 (s), 1581 (s), 1560 (m), 1523 (m), 1482 (s), 1397 (m), 1382 (s), 1336 (m), 1299 (s), 1268 (s), 1192 (w), 1175 (m), 1158 (m), 1098 (w), 1040 (m), 941 (s), 895 (m), 864 (w), 833 (w), 822 (m), 791 (m), 736 (s), 719 (s), 628 (m), 588 (w), 571 (m), 540 (m), 501 (m), 475 (w), 416 (w) cm^{-1}; elemental analysis calcd (%) for $C_{50}H_{50}CaF_2N_6O_{16}$: C 56.18, H 4.71, Ca 3.75, N 7.86; found: C 56.07, H 4.76, Ca 3.81, N 7.93.

$[Mn(cf)_2]\cdot 2.5H_2O$ (10): A mixture of $Mn(OAc)_2\cdot 4H_2O$ (0.25 mmol), ciprofloxacin hydrochloride (0.5 mmol), and water (7 mL) was stirred and adjusted to pH 11.5 with 2.5 M NaOH solution. The mixture was transferred and sealed into an 18-mL Teflon-lined autoclave, which was heated at 120 °C for 96 h. After the mixture had been allowed to slowly cool to room temperature, yellow blocks of **10** were filtered off, washed with distilled water, and dried at ambient temperature (yield: 74% based on Mn). IR (KBr): $\tilde{\nu}$ = 3385 (br), 3199 (m), 3028 (w), 2972 (w), 2918 (m), 2865 (w), 1622 (s), 1584 (s), 1557 (s), 1533 (s), 1485 (s), 1461 (m), 1439 (m), 1381 (s), 1334 (m), 1302 (s), 1276 (m), 1260 (s), 1222 (m), 1179 (m), 1117 (m), 1073 (w), 1035 (m), 1010 (s), 944 (s), 898 (m), 888 (s), 866 (w), 829 (s), 814 (m), 787 (m), 765 (w), 746 (s), 702 (m), 668 (m), 630 (m), 542 (w), 492 (m), 460 (w), 438 (w), 421 (w) cm^{-1}; elemental analysis calcd (%) for $C_{34}H_{39}F_2MnN_6O_{8.50}$: C 53.69, H 5.17, Mn 7.22, N 11.05; found: C 53.75, H 5.19, Mn 7.11, N 11.12.

[Co(cf)$_2$]·2.5H$_2$O (11): The preparation of **11** was similar to that of **10** except that Co(OAc)$_2$·4H$_2$O was used instead of Mn(OAc)$_2$·4H$_2$O. Orange blocks of **11** were obtained in 71% yield. IR (KBr): $\tilde{\nu}$ = 3385 (br), 3216 (m), 3027 (w), 3002 (w), 2970 (w), 2922 (m), 1622 (s), 1583 (s), 1559 (s), 1534 (m), 1486 (s), 1462 (m), 1383 (s), 1336 (m), 1304 (s), 1278 (m), 1261 (s), 1223 (m), 1180 (m), 1119 (m), 1073 (w), 1040 (m), 1010 (s), 946 (s), 899 (m), 889 (m), 855 (w), 829 (s), 813 (m), 788 (m), 749 (s), 703 (w), 668 (w), 632 (w), 542 (w), 496 (m), 461 (w), 445 (w), 427 (w) cm^{-1}; elemental analysis calcd (%) for $C_{34}H_{39}CoF_2N_6O_{8.50}$: C 53.41, H 5.14, Co 7.71, N 10.99; found: C 53.53, H 5.11, Co 7.75, N 10.92.

[Zn(cf)$_2$]·2.5H$_2$O (12): The preparation of **12** was similar to that of **10** except that Zn(OAc)$_2$·2H$_2$O was used instead of Mn(OAc)$_2$·4H$_2$O. Colorless blocks of **12** were obtained in 81% yield. IR (KBr): $\tilde{\nu}$ = 3367 (br), 3208 (m), 3027 (w), 3002 (w), 2971 (w), 2923 (m), 2840 (w), 1622 (s), 1582 (s), 1558 (s), 1533 (s), 1485 (s), 1461 (m), 1444 (w), 1382 (s), 1336 (m), 1302 (s), 1278 (m), 1260 (s), 1222 (m), 1179 (m), 1118 (m), 1073 (w), 1040 (m), 1029 (m), 1011 (s), 945 (s), 899 (m), 888 (s), 866 (w), 829 (s), 813 (m), 783 (m), 764 (w), 747 (s), 739 (m), 702 (m), 668 (m), 644 (w), 630 (m), 542 (m), 494 (m), 460 (w), 443 (w), 425 (w) cm^{-1}; elemental analysis calcd (%) for $C_{34}H_{39}F_2N_6O_{8.50}Zn$: C 52.96, H 5.10, N 10.90, Zn 8.48; found: C 53.08, H 5.07, N 10.86, Zn 8.53.

[Cd(cf)$_2$]·2.5H$_2$O (13): The preparation of **13** was similar to that of **10** except that Cd(NO$_3$)$_2$·4H$_2$O was used instead of Mn(OAc)$_2$·4H$_2$O. Colorless blocks of **13** were obtained in 77% yield. IR (KBr): $\tilde{\nu}$ = 3371 (br), 3154 (m), 3030 (w), 2981 (w), 2948 (w), 2921 (m), 2830 (w), 1620 (s), 1581 (s), 1557 (s), 1531 (s), 1488 (s), 1462 (m), 1442 (m), 1377 (s), 1333 (m), 1300 (s), 1275 (m), 1260 (s), 1222 (m), 1179 (m), 1117 (m), 1055 (m), 1019 (s), 943 (s), 897 (m), 887 (s), 828 (s), 812 (m), 787 (m), 766 (w), 744 (s), 702 (m), 668 (w), 629 (m), 542 (w), 493 (m), 460 (w), 441 (w), 423 (w) cm^{-1}; elemental analysis calcd (%) for $C_{34}H_{39}CdF_2N_6O_{8.50}$: C 49.92, H 4.80, Cd 13.74, N 10.27; found: C 49.84, H 4.85, Cd 13.79, N 10.33.

[Mg(cf)$_2$]·2.5H$_2$O (14): The preparation of **14** was similar to that of **10** except that Mg(NO$_3$)$_2$·6H$_2$O was used instead of Mn(OAc)$_2$·4H$_2$O. Colorless irregular blocks of **14** were obtained in 42% yield. IR (KBr): $\tilde{\nu}$ = 3378 (br), 3217 (m), 3027 (w), 2997 (w), 2965 (w), 2920 (m), 2841 (w), 1629 (s), 1590 (s), 1562 (s), 1538 (s), 1488 (s), 1461 (m), 1441 (w), 1386 (s), 1341 (m), 1307 (s), 1278 (m), 1261 (s), 1223 (m), 1180 (m), 1119 (m), 1037 (m), 1007 (s), 947 (s), 900 (m), 889 (s), 867 (w), 830 (s), 817 (m), 789 (m), 764 (w), 750 (s), 702 (m), 670 (m), 632 (m), 554 (w), 499 (m), 446 (w), 426 (w) cm^{-1}; elemental analysis calcd (%) for $C_{34}H_{39}F_2MgN_6O_{8.50}$: C 55.94, H 5.38, Mg 3.33, N 11.51; found: C 56.05, H 5.40, Mg 3.38, N 11.43.

TG analyses: The TG curve of compound **1** is shown in Figure S11a in the Supporting Information. The TG curve of **1** exhibits four stages of weight loss. The first weight loss of 4.52% lies in the temperature range of 135–185 °C, corresponding to the release of the non-coordinated and coordinated water molecules (calcd 4.68%). The second weight loss is 32.22% at 315– 420 °C; the third step is 23.65% from 420–500 °C, and the last step is 5.10% in the temperature range of 500–600 °C, all assigned to the decomposition of cf and 1,4-bdc ligands (calcd 61.11%). The residue is $BaCO_3$. The total weight loss (65.49%) is in agreement with the calculated value (65.79%).

The TG curve of compound **2** (see Figure S11b in the Supporting Information) shows a total weight loss of 71.23% in the temperature range of 125–635 °C, which agrees with the calculated value of 71.83%. The weight loss of 4.43% at 125–205 °C corresponds to the loss of the non-coordinated and coordinated water molecules (calcd 4.58%). The weight

Table 1. Crystal data and structure refinement for **1**–**14**.

	1	**2**	**3**	**4**	**5**	**6**	**7**
formula	$C_{42}H_{44}Ba_2F_2N_6O_{13}$	$C_{126}H_{130}F_6N_{18}O_{38}Sr_6$	$C_{51}H_{62}F_2Mn_2N_6O_{25}$	$C_{51}H_{62}Cd_2F_2N_6O_{25}$	$C_{25}H_{22}FMnN_3O_7$	$C_{25}H_{22}CoFN_3O_7$	$C_{25}H_{22}FN_3O_7Zn$
fw	1153.51	3144.20	1306.95	1421.87	550.40	554.39	560.83
space group	$P\bar{1}$	$P\bar{1}$	$P\bar{1}$	$P\bar{1}$	$P\bar{1}$	$P\bar{1}$	$P\bar{1}$
a [Å]	9.0295(18)	10.146(2)	12.043(2)	12.070(2)	9.953(2)	9.939(2)	9.817(2)
b [Å]	10.213(2)	16.320(3)	14.010(3)	14.005(3)	10.131(2)	10.043(2)	10.057(2)
c [Å]	12.034(2)	19.274(4)	17.876(4)	17.908(4)	12.793(3)	12.674(3)	12.858(3)
α [°]	98.22(3)	97.74(3)	71.79(3)	72.04(3)	107.23(3)	106.63(3)	107.49(3)
β [°]	101.58(3)	95.75(3)	87.39(3)	87.44(3)	107.81(3)	107.79(3)	108.28(3)
γ [°]	91.45(3)	95.05(3)	86.65(3)	87.12(3)	96.87(3)	97.09(3)	96.19(3)
V [Å^3]	1074.4(4)	3129.8(11)	2858.9(10)	2874.5(10)	1141.3(4)	1123.0(4)	1120.6(4)
Z	1	1	2	2	2	2	2
ρ_{calcd} [g cm^{-3}]	1.783	1.668	1.518	1.643	1.602	1.639	1.662
μ [mm^{-1}]	1.904	2.640	0.539	0.836	0.641	0.828	1.160
$R_1[I>2\sigma(I)]$[a]	0.0309	0.0517	0.0642	0.0540	0.0356	0.0419	0.0441
wR_2 (all data)[b]	0.0986	0.1618	0.1779	0.1328	0.1239	0.0859	0.0978

	8	**9**	**10**	**11**	**12**	**13**	**14**
formula	$C_{84}H_{106}F_4N_{12}O_{33}Zn_2$	$C_{50}H_{50}CaF_2N_6O_{16}$	$C_{34}H_{39}F_2MnN_6O_{8.50}$	$C_{34}H_{39}CoF_2N_6O_{8.50}$	$C_{34}H_{39}F_2N_6O_{8.50}Zn$	$C_{34}H_{39}CdF_2N_6O_{8.50}$	$C_{34}H_{39}F_2MgN_6O_{8.50}$
Fw	2018.55	1069.04	760.65	764.64	771.08	818.11	730.02
space group	*C*2/*m*	$P2_1/n$	$P2_1/c$	$P2_1$/c	$P2_1/c$	$P2_1/c$	$P2_1/c$
a [Å]	18.558(4)	9.5003(19)	5.9038(12)	5.9395(12)	5.9352(12)	5.7035(11)	6.0115(12)
b [Å]	25.388(5)	22.112(4)	21.855(4)	21.623(4)	21.626(4)	22.230(4)	21.616(4)
c [Å]	12.514(3)	11.869(2)	13.479(3)	13.302(3)	13.339(3)	13.644(3)	13.281(3)
α [°]	90	90	90	90	90	90	90
β [°]	127.51(3)	99.30(3)	100.59(3)	101.57(3)	101.45(3)	100.61(3)	101.20(3)
γ [°]	90	90	90	90	90	90	90
V [Å^3]	4677.4(16)	2460.5(9)	1709.5(6)	1673.7(6)	1678.0(6)	1700.4(6)	1692.9(6)
Z	2	2	2	2	2	2	2
ρ_{calcd} [g cm^{-3}]	1.433	1.443	1.478	1.517	1.526	1.598	1.432
μ [mm^{-1}]	0.610	0.214	0.460	0.588	0.807	0.717	0.127
$R_1[I>2\sigma(I)]$[a]	0.0751	0.0517	0.0421	0.0442	0.0408	0.0287	0.0531
wR_2 (all data)[b]	0.1829	0.1587	0.1331	0.1351	0.1216	0.0839	0.1532

[a] $R_1 = \Sigma||F_o|-|F_c||/\Sigma|F_o|$. [b] $wR_2 = \Sigma[w(F_o^2-F_c^2)^2]/\Sigma[w(F_o^2)^2]^{1/2}$.

loss of 66.80% at 325–635°C arises from the release of cf and 1,4-bdc ligands (calcd 67.25%). The residue is $SrCO_3$.

The TG curve of **3** is shown in Figure S12a in the Supporting Information. It gives a total weight loss of 88.91% in the range of 62–500°C, which agrees with the calculated value of 89.14%. The first weight loss is 13.74% in the temperature range of 62–140°C, which corresponds to the loss of all non-coordinated and coordinated water molecules (calcd 13.78%), and then the sample remains relatively stable in the temperature range of 140–252°C. The second weight loss is 18.90% from 252 to 370°C, and the third step is 56.27% from 370 to 500°C, both assigned to the decomposition of cf and bptc ligands (calcd 75.36%). The residue is MnO. The TG curve of compound **4** exhibits similar weight loss stages to those of compound **3** (see Figure S12b in the Supporting Information). In **4** the total weight loss (82.05%) is in agreement with the calculated value (81.94%).

The TG curve of **5** exhibits three weight loss stages in the temperature ranges 235–335 (3.92%), 345–410 (20.01%), and 410–510°C (62.87%) (see Figure S13a in the Supporting Information), corresponding to the release of cf and 1,3-bdc groups. The residue is MnO. The total weight loss (86.80%) is in good agreement with the calculated value (87.11%). The TG curves of compounds **6** and **7** exhibit similar weight loss stages to those of compound **5** (see Figure S13b and Figure S13c in the Supporting Information). For **6**, the total weight loss (86.30%) is in agreement with the calculated value (86.48%). For **7**, the total weight loss (85.99%) is in agreement with the calculated value (85.49%).

Table 2. Selected bond lengths [Å] for **1**–**14**.[a]

				1					
Ba1–O2A	2.637(2)	Ba1–O2	2.825(2)	Ba1–O3A	2.705(2)	Ba1–O1	2.826(2)	Ba1–O4B	2.722(2)
Ba1–O5	2.834(3)	Ba1–OW1	2.807(3)	Ba1–O4	2.849(3)				
				2					
Sr1–O13	2.494(3)	Sr1–O6	2.643(3)	Sr1–O14A	2.564(3)	Sr1–O4	2.670(3)	Sr1–O15	2.580(3)
Sr1–O8	2.713(3)	Sr1–OW1	2.639(3)	Sr1–O14	2.771(3)	Sr2–O4	2.490(3)	Sr2–OW2	2.632(3)
Sr2–O7	2.532(3)	Sr2–O5	2.653(3)	Sr2–O9	2.561(3)	Sr2–O13	2.696(3)	Sr2–O3B	2.632(3)
Sr2–O12B	2.759(3)	Sr3–O10	2.493(3)	Sr3–O2	2.592(4)	Sr3–O11	2.518(3)	Sr3–OW3	2.617(3)
Sr3–O1	2.535(3)	Sr3–O9	2.736(3)	Sr3–O12B	2.540(3)				
				3					
Mn1–O3	2.112(2)	Mn2–O9	2.142(3)	Mn1–O2A	2.161(2)	Mn2–O6	2.148(2)	Mn1–O11	2.169(3)
Mn2–O8	2.154(3)	Mn1–OW1	2.198(3)	Mn2–OW2	2.186(3)	Mn1–O13	2.200(3)	Mn2–O5B	2.203(2)
Mn1–O2	2.299(3)	Mn2–O5	2.240(3)						
				4					
Cd1–O11	2.249(4)	Cd2–O5B	2.216(3)	Cd1–O2A	2.264(3)	Cd2–O6	2.219(3)	Cd1–O13	2.268(4)
Cd2–O8	2.252(3)	Cd1–O3	2.271(3)	Cd2–OW2	2.286(3)	Cd1–OW1	2.272(5)	Cd2–O9	2.326(3)
Cd1–O2	2.330(4)	Cd2–O5	2.398(3)						
				5					
Mn1–O6A	2.1167(14)	Mn1–O2	2.1644(13)	Mn1–O3	2.1399(14)	Mn1–O4	2.2477(17)	Mn1–O7B	2.1471(12)
Mn1–O5	2.3789(13)								
				6					
Co1–O6A	2.0270(12)	Co1–O2	2.0890(18)	Co1–O3	2.0333(14)	Co1–O4	2.1935(16)	Co1–O7B	2.0743(16)
Co1–O5	2.2342(12)								
				7					
Zn1–O6A	1.9983(19)	Zn1–O4	2.094(3)	Zn1–O3	2.037(2)	Zn1–O7B	2.082(3)	Zn1–O2	2.085(3)
Zn1–O5	2.450(2)								
				8					
Zn1–O1	2.014(4)	Zn1–O3	2.047(3)	Zn1–O1A	2.014(4)	Zn1–O4	2.208(4)	Zn1–O3A	2.047(3)
Zn1–O4A	2.208(4)								
				9					
Ca1–O2A	2.2860(13)	Ca1–O4	2.3100(15)	Ca1–O2	2.2860(13)	Ca1–O3	2.3203(13)	Ca1–O4A	2.3100(15)
Ca1–O3A	2.3203(13)								
				10					
Mn1–O2A	2.1449(16)	Mn1–O3A	2.1562(13)	Mn1–O2	2.1449(16)	Mn1–N1B	2.3465(15)	Mn1–O3	2.1562(13)
Mn1–N1C	2.3465(15)								
				11					
Co1–O2A	2.0588(18)	Co1–O3A	2.0714(14)	Co1–O2	2.0588(18)	Co1–N1B	2.2410(18)	Co1–O3	2.0714(14)
Co1–N1C	2.2410(18)								
				12					
Zn1–O2A	2.0779(19)	Zn1–O3	2.0873(17)	Zn1–O2	2.0779(19)	Zn1–N1B	2.245(2)	Zn1–O3A	2.0873(17
Zn1–N1C	2.245(2)								
				13					
Cd1–O2	2.2694(18)	Cd1–O3	2.2881(14)	Cd1–O2A	2.2694(18)	Cd1–N1B	2.3594(17)	Cd1–O3A	2.2881(14)
Cd1–N1C	2.3594(17)								
				14					
Mg1–O2A	2.0389(15)	Mg1–O3	2.0477(14)	Mg1–O2	2.0389(15)	Mg1–N1B	2.2954(18)	Mg1–O3A	2.0477(14)
Mg1–N1C	2.2954(18)								

[a] Symmetry transformations used to generate equivalent atoms: for **1**: A = $-x,-y,-z$; B = $-x-1,-y,-z$; for **2**: A = $-x,-y+1,-z+1$; B = $x+1,y,z$; for **3**: A = $-x+1,-y,-z$; B = $-x,-y+2,-z-1$; for **4**: A = $-x+1,-y-1,-z+2$; B = $-x,-y+1,-z+1$; for **5**: A = $x,y-1,z$; B = $-x,-y+1,-z$; for **6** and **7**: A = $x,y+1,z$; B = $-x,-y-1,-z$; for **8**: A = $-x+1,y,-z+1$; for **9**: A = $-x+1,-y,-z+1$; for **10** and **14**: A = $-x+1,-y+1,-z+1$; B = $-x,y+1/2,-z+1/2$; C = $x+1,-y+1/2,z+1/2$; for **11**: A = $-x+1,-y+1,-z+1$; B = $x+1,-y+3/2,z+1/2$; C = $-x,y-1/2,-z+1/2$; for **12**: A = $-x,-y,-z$; B = $x-1,-y+1/2,z-1/2$; C = $-x+1,y-1/2,-z+1/2$; for **13**: A = $-x+1,-y+1,-z$; B = $-x,y+1/2,-z-1/2$; C = $x+1,-y+1/2,z+1/2$.

The TG curve of **8** exhibits four stages of weight loss (see Figure S14 in the Supporting Information). The first weight loss is 19.71% in the temperature range of 33–245°C, corresponding to the release of the non-coordinated water and 1,4-H_2bdc molecules (calcd 19.83%). The sample then remains relatively stable in the temperature range of 245–265°C. The second weight loss is 25.72% from 265–405°C; the third step is 12.35% from 405–495°C, and the last step is 33.79% in the temperature range of 495–590°C, all assigned to the decomposition of coordinated cf and 1,4-bdc ligands (calcd 72.11%). The residue is ZnO. The total weight loss (91.57%) is in agreement with the calculated value (91.94%).

The TG curve of **9** exhibits four stages of weight loss in the temperature ranges 45–170 (3.26%), 235–343 (18.11%), 343–449 (20.84%), and 449–575°C (51.77%) (see Figure S15 in the Supporting Information), corresponding to the release of non-coordinated water, cf, and 1,2-Hbdc groups. The residue is CaO. The total weight loss (93.98%) is in good agreement with the calculated value (94.75%).

The TG curve of **10** exhibits three stages of weight loss (see Figure S16a in the Supporting Information). The first weight loss is 5.80% in the temperature range of 40–130°C, corresponding to the release of non-coordinated water molecules (calcd 5.92%). The sample then remains relatively stable in the temperature range of 130–290°C, indicating the formation of stable nanosized channels. The second weight loss is 30.35% from 290–350°C, and the third step is 54.29% in the temperature range of 350–470°C, all assigned to the decomposition of cf ligands (calcd 84.75%). The residue is MnO. The total weight loss (90.44%) is in agreement with the calculated value (90.67%). The TG curves of compounds **11**, **12**, **13**, and **14** exhibit similar stages of weight loss to those of compound **10** (see Figure S16b–e in the Supporting Information). In **11**, the total weight loss (89.63%) is in agreement with the calculated value (90.20%). In **12**, the total weight loss (90.05%) is in agreement with the calculated value (89.44%). In **13**, the total weight loss (83.60%) is in agreement with the calculated value (84.13%). In **14**, the total weight loss (93.79%) is in agreement with the calculated value (94.48%).

Crystal structure determination: Intensity data were collected on a Rigaku R-AXIS RAPID IP diffractometer with $Mo_{K\alpha}$ monochromated radiation ($\lambda = 0.71073$ Å) at 293 K. Empirical absorption correction was applied. The structures of **1**–**14** were solved by the direct method and refined by the full-matrix least-squares method on F^2 with SHELXL-97 software.[24] All of the non-hydrogen atoms were refined anisotropically. The organic hydrogen atoms were generated geometrically; the aqua hydrogen atoms were located from difference maps and refined with isotropic temperature factors. A summary of the crystal data and structure refinement for compounds **1**–**14** is provided in Table 1. Selected bond lengths of **1**–**14** are listed in Table 2.

CCDC-268310 to CCDC-268323 contain the supplementary crystallographic data for this paper. These data can be obtained free of charge from the Cambridge Crystallographic Data Centre via www.ccdc.cam.ac.uk/data_request/cif.

Acknowledgements

The authors thank the National Natural Science Foundation of China (20371011) for financial support.

[1] a) S. R. Batten, R. Robson, *Angew. Chem.* **1998**, *110*, 1558; *Angew. Chem. Int. Ed.* **1998**, *37*, 1460; b) P. J. Hagrman, D. Hagrman, J. Zubieta, *Angew. Chem.* **1999**, *111*, 2798; *Angew. Chem. Int. Ed.* **1999**, *38*, 2638; c) A. J. Blake, N. R. Champness, P. Hubberstey, W. S. Li, M. A. Withersby, M. Schröder, *Coord. Chem. Rev.* **1999**, *183*, 117.

[2] a) B. Moulton, M. J. Zaworotko, *Chem. Rev.* **2001**, *101*, 1629; b) O. R. Evans, W. Lin, *Acc. Chem. Res.* **2002**, *35*, 511; c) X. C. Huang, J. P. Zhang, X. M. Chen, *J. Am. Chem. Soc.* **2004**, *126*, 13218; d) L. Carlucci, G. Ciani, D. M. Proserpio, *Coord. Chem. Rev.* **2003**, *246*, 247.

[3] a) A. Müller, S. K. Das, S. Talismanov, S. Roy, E. Beckmann, H. Bögge, M. Schmidtmann, A. Merca, A. Berkle, L. Allouche, Y. Zhou, L. Zhang, *Angew. Chem.* **2003**, *115*, 5193; *Angew. Chem. Int. Ed.* **2003**, *42*, 5039; b) C. D. Wu, C. Z. Lu, H. H. Zhuang, J. S. Huang, *J. Am. Chem. Soc.* **2002**, *124*, 3836; c) D. N. Dybtsev, H. Chun, K. Kim, *Angew. Chem.* **2004**, *116*, 5143; *Angew. Chem. Int. Ed.* **2004**, *43*, 5033; d) Y. Y. Niu, H. G. Zheng, H. W. Hou, X. Q. Xin, *Coord. Chem. Rev.* **2004**, *248*, 169; e) X. H. Bu, M. L. Tong, H. C. Chang, S. Kitagawa, S. R. Batten, *Angew. Chem.* **2004**, *116*, 194; *Angew. Chem. Int. Ed.* **2004**, *43*, 192.

[4] a) O. M. Yaghi, M. O'Keeffe, N. W. Ockwig, H. K. Chae, M. Eddaoudi, J. Kim, *Nature* **2003**, *423*, 705; b) S. Kitagawa, R. Kitaura, S. I. Noro, *Angew. Chem.* **2004**, *116*, 2388; *Angew. Chem. Int. Ed.* **2004**, *43*, 2334; c) C. N. R. Rao, S. Natarajan, R. Vaidhyanathan, *Angew. Chem.* **2004**, *116*, 1490; *Angew. Chem. Int. Ed.* **2004**, *43*, 1466; d) B. H. Ye, M. L. Tong, X. M. Chen, *Coord. Chem. Rev.* **2005**, *249*, 545.

[5] a) H. Li, M. Eddaoudi, M. O'Keeffe, O. M. Yaghi, *Nature* **1999**, *402*, 276; b) B. Chen, M. Eddaoudi, S. T. Hyde, M. O'Keeffe, O. M. Yaghi, *Science* **2001**, *291*, 1021; c) J. Kim, B. Chen, T. M. Reineke, H. Li, M. Eddaoudi, D. B. Moler, M. O'Keeffe, O. M. Yaghi, *J. Am. Chem. Soc.* **2001**, *123*, 8239; d) N. L. Rosi, M. Eddaoudi, J. Kim, M. O'Keeffe, O. M. Yaghi, *Angew. Chem.* **2002**, *114*, 294; *Angew. Chem. Int. Ed.* **2002**, *41*, 284; e) M. Eddaoudi, J. Kim, N. Rosi, D. Vodak, D. V. Wachter, M. O'Keeffe, O. M. Yaghi, *Science* **2002**, *295*, 469; f) N. L. Rosi, J. Eckert, M. Eddaoudi, D. T. Vodak, J. Kim, M. O'Keeffe, O. M. Yaghi, *Science* **2003**, *300*, 1127.

[6] a) S. S.-Y. Chui. S. M.-F. Lo, J. P. H. Charmant, A. G. Orpen, I. D. Williams, *Science* **1999**, *283*, 1148; b) S. M.-F. Lo, S. S.-Y. Chui, L. Y. Shek, Z. Y. Lin, X. X. Zhang, G. H. Wen, I. D. Williams, *J. Am. Chem. Soc.* **2000**, *122*, 6293.

[7] a) K. Barthelet, J. Marrot, D. Riou, G. Férey, *Angew. Chem.* **2002**, *114*, 291; *Angew. Chem. Int. Ed.* **2002**, *41*, 281; b) F. Millange, C. Serre, G. Férey, *Chem. Commun.* **2002**, 822; c) D. R. Xiao, Y. G. Li, E. B. Wang, S. T. Wang, Y. Hou, G. J. H. De, C. W. Hu, *Inorg. Chem.* **2003**, *42*, 7652.

[8] a) X. M. Chen, G. F. Liu, *Chem. Eur. J.* **2002**, *8*, 4811; b) X. M. Zhang, M. L. Tong, M. L. Gong, X. M. Chen, *Eur. J. Inorg. Chem.* **2003**, 138; c) D. R. Xiao, Y. Xu, Y. Hou, E. B. Wang, S. T. Wang, Y. G. Li, L. Xu, C. W. Hu, *Eur. J. Inorg. Chem.* **2004**, 1385.

[9] a) R. Cao, D. F. Sun, Y. C. Liang, M. C. Hong, K. Tatsumi, Q. Shi, *Inorg. Chem.* **2002**, *41*, 2087; b) J. H. Luo, M. C. Hong, R. H. Wang, R. Cao, L. Han, D. Q. Yuan, Z. Z. Lin, Y. F. Zhou, *Inorg. Chem.* **2003**, *42*, 4486.

[10] a) R. X. Yuan, R. G. Xiong, B. F. Abrahams, G. H. Lee, S. M. Peng, C. M. Che, X. Z. You, *J. Chem. Soc. Dalton Trans.* **2001**, 2071; b) Z. F. Chen, R. G. Xiong, J. L. Zuo, Z. Guo, X. Z. You, H. K. Fun, *J. Chem. Soc. Dalton Trans.* **2000**, 4013; c) Z. F. Chen, R. G. Xiong, J. Zhang, X. T. Chen, Z. L. Xue, X. Z. You, *Inorg. Chem.* **2001**, *40*, 4075; d) Z. F. Chen, B. Q. Li, Y. R. Xie, R. G. Xiong, X. Z. You, X. L. Feng, *Inorg. Chem. Commun.* **2001**, *4*, 346; e) R. X. Yuan, R. G. Xiong, Z. F. Chen, P. Zhang, H. X. Ju, Z. Dai, Z. J. Guo, H. K. Fun, X. Z. You, *J. Chem. Soc. Dalton Trans.* **2001**, 774.

[11] a) C. Chulvi, M. C. Muñoz, L. Perelló, R. Ortiz, M. I. Arriortua, J. Via, K. Urtiaga, J. M. Amigó , L. E. Ochando, *J. Inorg. Biochem.* **1991**, *42* 133; b) M. Ruiz, R. Ortiz, L. Perelló, A. Castiñeiras, M. Quiró, *Inorg. Chim. Acta* **1993**, *211*, 133; c) M. Ruiz, R. Ortiz, L. Perelló, J. Latorre, J. Server-Carrió, *J. Inorg. Biochem.* **1997**, *65*, 87; d) M. Ruiz, L. Perelló, R. Ortiz, A. Castiñeiras, C. Maichle-Mössmer, E. Cantón, *J. Inorg. Biochem.* **1995**, *59*, 801; e) B. Macías, M. V. Villa, I. Rubio, A. Castiñeiras, J. Borrás, *J. Inorg. Biochem.* **2001**, *84*, 163.

[12] a) G. Mendoza-Díaz, L. M. R. Martinez-Aguilera, R. Perez-Alonso, *Inorg. Chim. Acta* **1987**, *138*, 41; b) G. Mendoza-Díaz, L. M. R. Martínez-Aguilera, R. Moreno-Esparza, K. H. Pannell, F. Cervantes-Lee, *J. Inorg. Biochem.* **1993**, *50*, 65; c) M. Ruiz, R. Ortiz, L. Perelló, S. García-Granda, M. R. Díaz, *Inorg. Chim. Acta* **1994**, *217*, 149; d) M. Ruiz, L. Perelló, J. Server-Carrió, R. Ortiz, S. García-Granda, M. R. Díaz, E. Cantón, *J. Inorg. Biochem.* **1998**, *69*, 231; e) E. Y.

Bivián-Castro, F. Cervantes-Lee, G. Mendoza-Díaz, *Inorg. Chim. Acta* **2004**, *357*, 349.

[13] a) D. T. W. Chu, P. B. Fernandes, in *Advances in Drug Research, Vol. 21* (Ed.: B. Testa), London, Academic Press, **1991**, pp. 39–144; b) *Martindale, The Extra Pharmacopeia*, 30th ed. (Ed.: J. E. F. Reynolds), The Pharmaceutical Press, London, **1993**, pp. 145–147; c) O. Paulsen, *Drugs Today* **1987**, *23*, 269; d) H. C. Neu, *Am. J. Med.* 1987, 82, 395.

[14] I. Turel, *Coord. Chem. Rev.* **2002**, *232*, 27.

[15] a) N. Jiménez-Garrido, L. Perelló, R. Ortiz, G. Alzuet, M. González-Álvarez, E. Cantón, M. Liu-González, S. García-Granda, M. Pérez-Priede, *J. Inorg. Biochem.* **2005**, *99*, 677; b) P. Drevenšek, T. Zupancic, B. Pihlar, R. Jerala, U. Kolitsch, A. Plaper, I. Turel, *J. Inorg. Biochem.* **2005**, *99*, 432; c) M. P. López-Gresa, R. Ortiz, L. Perelló, J. Latorre, M. Liu-González, S. García-Granda, M. Pérez-Priede, E. Cantón, *J. Inorg. Biochem.* **2002**, *92*, 65; d) I. Turel, A. Golobiè, A. Klavžar, B. Pihlar, P. Buglyó, E. Tolis, D. Rehder, K. Sepcic, *J. Inorg. Biochem.* **2003**, *95*, 199.

[16] a) S. C. Wallis, L. R. Gahan, B. G. Charles, T. W. Hambley, *Polyhedron* **1995**, *14*, 2835; b) I. Turel, I. Leban, N. Bukovec, *J. Inorg. Biochem.* 1994, 56, 273; c) I. Turel, L. Goliè, O. L. Ruiz Ramirez, *Acta Chim. Slov.* **1999**, *46*, 203; d) S. C. Wallis, L. R. Gahan, B. G. Charles, T. W. Hambley, P. A. Duckworth, *J. Inorg. Biochem.* **1996**, *62*, 1; e) D. K. Saha, S. Padhye, C. E. Anson, A. K. Powell, *Inorg. Chem. Commun.* **2002**, *5*, 1022.

[17] a) L. L. Shen, A. G. Pernet, *Proc. Natl. Acad. Sci. USA* **1985**, *82*, 307; b) L. L. Shen, J. Baranowski, A. G. Pernet, *Biochemistry* **1989**, *28*, 3879; c) L. L. Shen, W. E. Kohlbrenner, D. Weigl, J. Baranowski, *J. Biol. Chem.* **1989**, *264*, 2973.

[18] a) J. Robles, J. Martín-Polo, L. Álvarez-Valtierra, L. Hinojosa, G. Mendoza-Díaz, *Met.-Based Drugs* **2000**, *7*, 301; b) C. Sissi, E. Perdona, E. Domenici, A. Feriani, A. J. Howells, A. Maxwell, M. Palumbo, *J. Mol. Biol.* **2001**, *311*, 195; c) N. Ramirez-Ramirez, G. Mendoza-Díaz, F. Gutiérrez-Corona, M. Pedraza-Reyes, *J. Biol. Inorg. Chem.* **1998**, *3*, 188.

[19] a) X. L. Wang, C. Qin, E. B. Wang, Y. G. Li, C. W. Hu, L. Xu, *Chem. Commun.* **2004**, 378; b) X. L. Wang, C. Qin, E. B. Wang, L. Xu, Z. M. Su, C. W. Hu, *Angew. Chem.* **2004**, *116*, 5146; *Angew. Chem. Int. Ed.* **2004**, *43*, 5036; c) C. Qin, X. L. Wang, L. Carlucci, M. L. Tong, E. B. Wang, C. W. Hu, L. Xu, *Chem. Commun.* **2004**, 1876.

[20] a) Y. Hou, S. T. Wang, E. H. Shen, E. B. Wang, D. R. Xiao, Y. G. Li, L. Xu, C. W. Hu, *Inorg. Chim. Acta* **2004**, *357*, 3155; b) S. V. Ganesan, S. Natarajan, *Inorg. Chem.* **2004**, *43*, 198.

[21] a) M. Kondo, T. Joshitomi, K. Seki, H. Matsuzaka, S. Kitagawa, *Angew. Chem.* **1997**, *109*, 1844; *Angew. Chem. Int. Ed. Engl.* **1997**, *36*, 1725; b) K. N. Power, T. L. Hennigar, M. J. Zaworotko, *New J. Chem.* **1998**, *22,* 177; c) L. Carlucci, G. Ciani, P. Macchi, D. M. Proserpio, S. Rizzato, *Chem. Eur. J.* **1999**, *5*, 237; d) S. R. Batten, B. F. Hoskins, R. Robson, *Chem. Eur. J.* **2000**, *6*, 156.

[22] D. N. Dybtsev, . H. Chun, S. H. Yoon, D. Kim, K. Kim, *J. Am. Chem. Soc.* **2004**, *126*, 32.

[23] a) J. Tao, Y. Zhang, M.-L. Tong, X.-M. Chen, T. Yuen, C. L. Lin, X. Y. Huang, J. Li, *Chem. Commun.* **2002**, 1342; b) H.-J. Chen, Z.-W. Mao, S. Gao, X.-M. Chen, *Chem. Commun.* **2001**, 2320; c) C.-M. Liu, S. Gao, H.-M. Hu, X. L. Jin, H.-Z. Kou, *J. Chem. Soc. Dalton Trans.* **2002**, 598.

[24] a) G. M. Sheldrick, SHELXS 97, Program for Crystal Structure Solution, University of Göttingen (Germany), **1997**; b) G. M. Sheldrick, SHELXL 97, Program for Crystal Structure Refinement, University of Göttingen (Germany), **1997**.

Received: May 17, 2005
Published online: August 10, 2005

